Discovery of a Devonian mafic magmatism on the western border of the Murzuq basin (Saharan metacraton): Paleomagnetic dating and geodynamical implications

Mohammed El Messaoud Derder, Said Maouche, Jean-Paul Liégeois, Bernard Henry, Mohamed Amenna, Aziouz Ouabadi, Hervé Bellón, Olivier Bruguier, Boualem Bayou, Rafik Bestandji, et al.

Discovery of a Devonian mafic magmatism on the western border of the Murzuq basin (Saharan metacraton): paleomagnetic dating and geodynamical implications.

M.E.M. Derder [1*], S. Maouche [1], J.P. Liégeois [2], B. Henry [3], M. Amenna [1], A. Ouabadi [4], H. Bellon [5], O. Bruguier [6], B. Bayou [1], R. Bestandji [1], O. Nouar [1,] H. Bouabdallah [1+], M. Ayache [1] and M. Beddiaf [7]

[1] *CRAAG, B.P. 63, Bouzaréah 16340 Alger, Algeria.*

[2] Geodynamics and Mineral Resources, *Royal Museum for Central Africa, B-3080 Tervuren, Belgium.*

[3] *Paléomagnétisme, Institut de Physique du Globe de Paris, Sorbonne Paris Cité, Univ. Paris Diderot and UMR 7154 CNRS, 4 avenue de Neptune, 94107 Saint-Maur cedex, France.*

[4] *Laboratoire "Géodynamique, Géologie de l'Ingénieur et Planétologie", FSTGAT / USTHB, BP 32, El-Alia Bab Ezzouar, 16111 Alger, Algeria.*

[5] *Université Européenne de Bretagne, UMR 6538 Domaines Océaniques, IUEM, Université de Bretagne Occidentale, Place Nicolas Copernic, 29280 Plouzané, France*

[6] *Géosciences Montpellier, Université de Montpellier UMR-CNRS 5243, 34095 Montpellier, France.*

[7] *Office National du Parc Culturel du Tassili N'ajjer, Djanet, Algeria*

* Corresponding author *Tel : +213 21 90 44 54 ; Fax : +213 21 90 44 58,* m.e.m.derder@gmail.com

\+ Now at geoexplo: www.geoexplo.dz

Email m.e.m.derder@gmail.com (M.E.M. Derder); said.maouche@gmail.com (S. Maouche); jean-paul.liegeois@africamuseum.be (J.P. Liégeois); henry@ipgp.fr (B. Henry); mohamed20_dz@yahoo.fr (M. Amenna); ouabadi@yahoo.fr (A. Ouabadi); herve.bellon@univ-brest.fr (H. Bellon); bruguier@gm.univ-montp2.fr (O. Bruguier); bbayou57@yahoo.fr (B. Bayou); bestandjirafik@gmail.com (R. Bestandji); obnouar@hotmail.com (O. Nouar); geoexplodz@gmail.com (H. Bouabdallah); mohamedayache62@yahoo.fr (M. Ayache); mbeddiaf@hotmail.com (M. Beddiaf).

Abstract

Keywords: Basic magmatism, Isotopic (K-Ar, U-Pb) dating, paleomagnetic dating, Devonian, Murzuq craton, Saharan metacraton

Abstract

Intraplate deformation is most often linked to major stress applied on plate margins. When such intraplate events are accompanied by magmatism, the use of several dating methods integrated within a multidisciplinary approach can bring constraints on the age, nature and source mobilized for generating the magma and in turn on the nature of the intraplate deformation. This study focuses on the large gabbro Arrikine sill (35 km in extension) emplaced within the Silurian sediments of the western margin of the Murzuq cratonic basin in southeastern Algeria. Its emplacement is dated during the early Devonian (415-400 Ma) through the determination of a reliable paleomagnetic pole by comparison with the Gondwana Apparent Polar Wander Path (APWP). This age can be correlated with deep phreatic eruptions before Pragian time thought to be at the origin of sand injections and associated circular structures in Algeria and Libya. For the sill, the K-Ar age of 325.6 ± 7.7 Ma is related to a K-rich aplitic phase that has K-enriched by more than 20% the Devonian gabbro. Laser-ICP-MS U-Pb method dates only inherited zircons mostly at c. 2030 Ma with additional ages at c. 2700 Ma and younger ones in the 766-598 Ma age range. The Arrikine sill is a high-Ti alkaline gabbro having the geochemical composition of a hawaiite akin to several intraplate continental and oceanic provinces, including the contemporaneous Aïr ring complexes province in Niger, but also to the Mauna Loa volcano in Hawaii. This peculiar composition akin to that of the contemporaneous Aïr province is in agreement with a lower Devonian age for the Arrikine sill.

The lower Devonian Arrikine sill emplacement is related to a “Caledonian” transtensive reactivation of the western metacratonic boundary of the Murzuq craton. This event also generated in the Saharan platform the so-called "Caledonian unconformity" of regional extension, the Aïr ring complexes and magmatic rocks that produced sand injections. It could be related to rifting of the Hun terranes that occurred at the plate margin to the north (Stampfli and Borel, 2002, Blackey, 2008 and references therein). The mid-Carboniferous (c. 326 Ma) reactivation corresponds to Variscan compression on NW Africa generating aplitic fluids, but also to the major "Hercynian unconformity" of regional extension. The generation of the Arrikine magma is attributed to partial melting through adiabatic pressure release of uprising asthenosphere along tectonically reactivated mega-shear zones, here bordering the relictual Murzuq craton enclosed in the Saharan metacraton.

1. Introduction

The Murzuq basin located in central North Africa, in Algeria, Libya and Niger (Fig. 1) is a key area within the Saharan metacraton, being located on a relictual cratonic nucleus, the Murzuq craton (Liégeois et al., 2013). It is one of the largest cratonic sedimentary basins of the Saharan platform, filled by different Phanerozoic series covered by a very large sandy desert, the Murzuq edeyen or erg. On its western border, we discovered a very large sill of mafic rocks interbedded in the Silurian sedimentary series belonging to the so-called Tassilis series. The sedimentary sequences unconformably rest on the late-Neoproterozoic Pan-African basement of the Tuareg Shield (Fig. 2). Known post-Pan-African magmatism in the In-Ezzane area is limited to Cenozoic lava flows (2.86 ± 0.07 Ma; Yahiaoui et al., 2014). Around the Murzuq basin, several large Cenozoic volcanic areas are known: Hoggar, Tibesti, Libyan basaltic fields (Liégeois et al., 2005; Fezaa et al., 2010). On the southwestern border of the Murzuq basin in Niger (between 11°53' E/22°27' N and 12°04' E/ 21°53' N), Paleozoic dolerites are mapped on the "Carte géologique du Sahara central" (Lelubre et al., 1962). These dolerites seem to be interbedded between Silurian and Devonian sedimentary sequences and correspond to a very large volume of mafic rocks (the biggest outcrop is indicated to be 90 km long on this map). Several hundred kilometers far to the west and southwest of In-Ezzane, Lower Carboniferous basic intrusions (Djellit et al., 2006; Derder et al., 2006) in the Tin Serririne basin and Devonian ring complexes in Aïr region (Black et al., 1967, Moreau et al., 1994) have been evidenced. In addition, Moreau et al. (2012) suggested that three areas with "sand injections", which generated circular structures along the Murzuq basin boundaries during lower Devonian, could be related to deep phreatic eruption before Pragian times (Lower Devonian, 407-410 Ma). One of these structures is very close to the sill in the In-Ezzane area (Fig. 1A). We note that the In-Ezzane circular structures proposed to be meteoritic impacts (Bonin et al., 2011; Reimold and Koeberl, 2014) are located more to the West, within the Ordovician sandstones.

Such an intraplate magmatism is a key event for understanding the geodynamical evolution of the Saharan platform. The aim of this paper is to date this event and to determine its different implications.

2. Geological setting

The Murzuq Basin is the principal feature of Central Sahara. This basin lies across Libya, Algeria and Niger. From a geomorphological point of view, this intracratonic sedimentary basin can be described as an enormous flat hollow of approximately 900 km in

diameter from Libya in the north to Niger in the south. This basin is filled by different Phanerozoic series covered by a very large sandy desert (the “Murzuq edeyen or erg"). The main morphological units of this basin consist of plateaus, oueds and sand dunes cover. The Tassili-n-Ajjer (Algeria) and Djado (Niger) uplifted plateaus constitute the southwestern and southern margins of this basin. Primary geological formations dip gently from the flanks towards the basin centre in a concentric pattern. In the In Djerane and Tadrart areas (Figs. 1 and 2), the different Paleozoic series (Cambro-Ordovician, Silurian, Devonian, Carboniferous and Permian – Henry et al., 2014) outcrop in several trenches of oueds, which produce remarkable rock cliffs (Fig. 2).

To the west, the Murzuq craton is bordered by its metacratonic margin, corresponding to the Djanet terrane, made of greenschist Ediacaran sediments (Fezaa et al., 2013) crosscut by 575-545 Ma old high-level plutonic bodies, batholiths, plutons and dyke swarms, (Fezaa et al., 2010). Further west, on the other side of a major NW-SE trending shear zone, the Edembo terrane resulted from a stronger intracontinental metacratonic reactivation that generated amphibolite-facies migmatitic gneisses and aluminous granitoids during the same period (c. 568 Ma; Fezaa et al., 2010). This intracontinental reactivation (575-545 Ma metacratonization) occurred to the east of the Raghane mega-shear zone (western boundary of the Saharan metacraton; Abdelsalam et al., 2002) in a region previously stable, that was covered by sediments deriving from the more western Tuareg Shield in the 595-575 Ma time span (Fezaa et al., 2010). These metacratonic reactivations occurred mostly along pre-existing Eburnean (c. 2 Ga) lithospheric-scale terrane boundaries, along the Murzuq craton, of probable Archean age (Fezaa et al., 2010).

These metacratonic zones were reactivated during the Mesozoic, with deposition of several thousand meters of sediments in troughs, and during the late Cenozoic, with the emplacement of the In-Ezzane basaltic field (Liégeois et al., 2013). The Phanerozoic sediments of the Murzuq basin are located to the East, partly resting on the Murzuq metacratonic margin, the Djanet terrane.

The Arrikine area consists of a monoclinal structure dipping 6° toward E to ENE. This structural orientation gradually changes. The Murzuq geological map (Geological Map of Libya, 1985) shows that its borders, including Cretaceous levels, were uplifted and slightly tilted. Very locally, folding has been observed in the In-Ezzane area (Amenna et al., 2014), probably related to far-field effects of the Hercynian orogeny (Haddoum et al., 2001), again reactivating the metacratonic structures.

In this area, we discovered a large sill of mafic rocks (maximum observed NNW-SSE outcrop extension of about 35 km) interbedded in Silurian sediments (Fig. 2). The current description of the local stratigraphy (Freulon, 1964; Bellini and Massa, 1980; Legrand, 2000; Ghienne et al., 2013), together with the published maps of this area, do not mention any occurrence of mafic rocks.

The sill intruded the upper member of the *Oued In Djerane Formation*, mainly made of shales. This upper member displays signs of a more marine environment than the underlying levels, but in its top part, presents facies that are more and more regressive (Legrand, 2000). It is overlain by the detritic *Acacus Formation*. The host-rocks constituting the roof of the sill are affected by a contact metamorphism.

3. Petrography and mineralogy

The Arrikine sill (Fig. 2) has a maximum thickness of c. 250 m and is dipping gently to the ENE similarly to the host-rocks series. The Silurian host-rocks, both at the floor and roof of the sill, show local folding due to the intrusion. Farther from the intrusion, in the Ordovician series, deformations become brittle. The sill is constituted of a pyroxene-rich gabbro. On its borders, it is light gray in color due to a strong weathering, while in the other parts, it is dark in appearance and not or slightly altered. These dark-facies rocks are medium-grained gray-green gabbros. The main mineral is plagioclase appearing as large lengthened intertwined laths. The mafic mineral assemblage is dominated by granular clinopyroxene. Minor constituents are thin laths of biotite associated with oxides, few small quartz grains and relatively large granules of opaque minerals. Weathering renders plagioclase brownish in color and is at the origin of the incomplete replacement of some pyroxene by chlorite.

Microprobe analyses (Table 1) confirm that the magmatic plagioclase is a labrador (An_{55}), the pyroxene a diopside, the presence of biotite and apatite and that the oxides are ilmenite and magnetite. The biotite is particularly rich in TiO_2 (c. 7%), which is also a characteristic of the biotite from the Iskou ring complex in Aïr (Léger, 1985). These analyses also show that Fe-Mg minerals are often altered but above all, that an aplitic component is present and is represented by small spots of K-feldspar, with diverse K compositions ranging from 2 wt % to 15 wt %. This K enrichment is accompanied by a Ba-enrichment (Table 1) developed within acid plagioclase (An_{13-17}), two minerals that cannot be in equilibrium with the gabbroic magma. The development of this phase enriched in K and Ba, has consequences for the whole rock geochemistry and its K-Ar dating (see below).

4. Isotopic dating

4.1 K/Ar geochronology

Analyses were done by one of us (H.B) at the K-Ar dating platform of UMR 6538 "Domaines Océaniques" CNRS, UBO at Brest.

4.1.1 Analytical procedure

This sample of gabbro (AF-ALG/Dj-Site58 from site 58 – Fig. 2) was also considered for dating on a whole-rock fraction made of grains 0.3 to 0.15 mm in size, prepared after hand-crushing and sieving of the solid rock, then cleaned using ultrapure water. One aliquot of grains was powdered in an agate grinder. Then two independent dissolutions of 80 mg of powdered sample were realized in two well-sealed synthetic bottles using 4 cm^3 of hydrofluoric acid at a temperature of 80°C for 8 hours. K content of the two HF solutions was determined by Atomic Absorption Spectrometry after dilution (1/2500).

A second aliquot of grains was reserved for under vacuum extraction of all gases by heating in a molybdenum crucible, using a high frequency generator. Cleaning of active gases from the whole extracted gases was realized during and after their extraction by gettering on hot titanium sponge contained in three quartz traps successively activated when their temperature was decreasing from 800°C to the ambient one during 10 minutes. The final step was the ultra-purification using an Al-Zr SAES getter.

Isotopic composition of argon and concentration of $^{40}Ar_R$ were measured in a stainless steel mass spectrometer with a 180° geometry. Isotopic dilution was realized during the fusion step, using precise concentrations of ^{38}Ar buried as ions in aluminium targets (Bellon et al., 1981).

A huge degasing of grains was observed and measured for the two first extractions from 0.4 to 0.3 g of sample and led to a long and difficult purification of argon; consequently it was less easy to reduce the effects of signal evolution through time . Two complementary extractions of gases from significantly lighter weights (0.07 and 0.06 g) have permitted to restore better conditions for purification and for isotopic analysis.

4.1.2 Data

Resulting data of the four extractions and isotopic analyses are presented in Table 2. Ages are calculated using Steiger and Jäger's (1977) constants and errors following the equation of Cox and Dalrymple (1967).

4.1.3 Interpretation

A mean age of 325.6 ± 7.7 Ma results from the analyses, i.e. a Serpukhovian age (from uppermost Visean to upper Bashkirian, if taking error margins into account). The Silurian age of the host sedimentary series questions the significance of the K-Ar age particularly when considering the huge degassing of samples under vacuum that may indicate the effects of secondary processes that affected the Arrikine sill.

Such a result points to an event occurring during the Variscan period. Therefore, it is legitimate to raise the question whether a geochemical remobilization of the sill, leading to a potassium and barium enrichment in the plagioclases (Table 1), has occurred. This alteration could have been promoted by cryptocirculations of fluids (supposed hot but not exactly known) that may have reset the K-Ar system by complete external diffusion of radiogenic ^{40}Ar. Following such a hypothesis, the 325.6 Ma age marks the time to which the gabbro should have been rejuvenated during the Variscan evolution.

4.2 U-Pb geochronology

4.2.1 Analytical procedure

Zircons were separated from 4 kg of rocks and were subsequently processed according to standard technique (e.g. Bosch et al., 1996), including magnetic separation and careful hand-picking under a binocular microscope. U-Pb dating on zircon was performed by laser ablation sector field ICP-MS at Geosciences Montpellier (France). The ICP-MS (ThermoFinnigan Element XR high resolution) was coupled to a Lambda Physik CompEx 102 excimer laser generating 15 ns duration pulses of radiation at a wavelength of 193 nm. Data were acquired at low resolution ($\Delta M/M = 300$) in the fast electrostatic scan mode. Signals were measured in pulse counting mode using 3 points per peaks and a 20% mass window. A pre-ablation step consisting of 7 pulses was applied to clean the sample surface. The acquisition step began with 15 s of gas blank measurement followed by 45 s of laser ablation at a frequency of 4 Hz with a spot size of 26 μm and an energy density of 10 J/cm^2. Measured isotopic ratios were monitored with reference to the G91500 zircon standard with a ^{206}Pb/^{238}U ratio of 0.17917 and a ^{207}Pb/^{206}Pb ratio of 0.07488 equivalent to ages of 1062 Ma and 1065 Ma, respectively (Wiedenbeck et al., 1995). The standard was measured four times each five unknowns in a sequence of 2 standards, 5 unknowns and 2 standards (see Bosch et al., 2011 for details). Analytical data are plotted and ages calculated using the IsoplotEx

program (Ludwig 2000). Analyses in Table 3 and in the Concordia plots are ±1σ errors and uncertainties in ages quoted in the text are given at ±2σ.

4.2.2 Results

Only 17 zircons were recovered, which is not so surprising in a basic rock. They display a large range of shapes and colors, indicating they do not form a homogeneous population. Most grains are subhedral to rounded, translucent and colorless to pink in color. Although some grains have euhedral shapes, the variety of shapes and the occurrence of rounded grains indicate that most grains may have been snatched from the country rocks, which possibly include a detrital component. Reported in the Concordia diagram (Fig. 3), analyzed grains display a wide range of ages, from Neoproterozoic to Archean, ranging from, 598±14 Ma to 2707±38 Ma (2σ, see Table 3). The main population is Paleoproterozoic with a mean age of around 2030 Ma (n= 7). The Neoproterozoic population is dominated by a coherent group of four grains plotting concordantly at *c.* 682 Ma, while other grains are concordant at 766, 632 and 598 Ma. Lastly the recovered zircon population includes a homogeneous Archean component dated at *c.* 2700 Ma.

4.2.3 Interpretation

The Arrikine sill cannot be older than the intruded Silurian sediments The dated zircons are therefore xenocrysts and not new minerals crystallized within the sill. This agrees with its low-silica geochemical composition and high temperature of crystallization, conditions during which the zircon saturation is very rarely attained (Watson and Harrison, 1983; Boehnke et al., 2013). The inherited zircons can have been incorporated in the Arrikine magma by incorporating (1) unmelted zircons from the source, (2) zircons from the basement during its ascent or (3) zircons from the Ediacaran or Paleozoic sediments during its final emplacement, these possibilities being not mutually exclusive.

Incorporating unmelted zircon crystals from the source is unlikely, again because such magmas are far from zircon saturation and are thus efficient to dissolve zircon (Watson and Harrison, 1983). Moreover, the source of the Arrikine gabbro (the mantle or the lower mafic crust) itself most probably bears very few zircons for the same reason.

The ages of the inherited zircons in the Arrikine gabbro (0.6, 0.63, 0.68, 2.03 and 2.7 Ga) match those of the detrital zircons from the Ediacaran sediments of the Djanet terrane, just to the west and probably present at depth below the Arrikine area (Fezaa et al., 2010). However, 2.7 Ga zircons are, strictly speaking, not present in these Ediacaran sediments (only 2.65 and 2.8 Ga old zircons are present). In addition, it is noteworthy that they bear other age

peaks, especially at 0.7, 1.9 and 2.5 Ga, which are not present in the Arrikine sill. The source of these sediments is Central Hoggar, especially its closest eastern part, explaining that some samples have a proximal immature source with few detrital zircon ages (Fezaa et al., 2010; 2013). So, the Ediacaran sediments could have provided some of the inherited zircons in the Arrikine sill, but other sources should be found.

The detrital zircons from the Tassilis Ordovician sandstones just to the West (Linnemann et al., 2011) display much more numerous age peaks. These sediments are considered as deriving from sources located all over West Africa and even Amazonia (Linnemann et al., 2011). However, the 2.7 Ga age is systematically absent. Incorporation of detrital zircons from these Ordovician mature sediments is thus not favored. The same conclusion can be reached for the Silurian series in which the Arrikine sill intruded. Its source is also distal and it is made of shales whose fine granulometry does not favor the presence of zircons.

The basement is not outcropping in the Easternmost Hoggar. The oldest known rocks are the Ediacaran sediments, metamorphosed in the greenschist facies (Djanet terrane) or migmatized in the amphibolite facies (Edembo terrane), intrusive and subvolcanic rocks being younger (Fezaa et al., 2010). Ediacaran magmatic rocks could have had extracted material but few old ages have been measured in their zircons. The Tin Amali dyke swarm for example provided a 2090 ±40 Ma age (Fezaa et al., 2010) for an inherited component. This age is not present in the detrital zircon age spectrum of the Ediacaran sediments and is likely to be related to the age of one basement component. More information can be obtained from the Nd isotopes. The mean T_{DM} model ages for the various magmatic bodies (batholith, pluton, and dyke swarm in the 575-545 Ma age range) fall in the 1.6-1.8 Ga age interval (Fezaa et al., 2010). This points to a Paleoproterozoic and/or Archean basement in the area. More to the west, but still to the east of the Raghane shear zone that constitutes the western boundary of the Saharan metacraton, the basement of the Aouzegueur terrane (the third Eastern Hoggar terrane; Fig. 1A) has been dated at 1918 ± 5 Ma (LA-ICP-MS U-Pb zircon age; Nouar et al., 2011). This basement is intruded by various granitoids close to the Raghane shear-zone at c. 790 Ma, c. 590 and c. 550 Ma (Henry et al., 2009; Nouar et al., 2011). All these ages do not correspond to the inherited zircons dated in the Arrikine sill.

So few informations are available on the basement below the Arrikine sill. Nd isotopes indicate that the basement is Paleoproterozoic and/or Archean in age and an inherited zircon point to an age of 2090 ± 40 Ma. On the other side, the Arrikine inherited zircons have two well-defined old ages at 2698 ± 22 Ma (3 zircons) and 2028 ± 15 Ma (7 zircons) with no other

zircons older than 1 Ga. These zircons can be considered as having been snatched from the underlying basement, but in very small quantities due to the low viscosity of this magma, and not from the superficial sediments that bear many ages but these ones. On the other hand, the younger inherited zircons, at 682 ±7 Ma (4 zircons), 632 ±10 Ma (1 zircon) and 598 ±15 Ma (1 zircon) could be sourced from the Ediacaran sediments that derived from the erosion of Neoproterozoic units close to the Raghane shear zone.

The Arrikine sill, through its inherited zircons, is thus currently the best probe for getting information on the basement of the Murzuq craton, at least of its western boundary, indicating the existence of Archean (c 2.7 Ga) and Paleoproterozoic (c. 2.03 Ga) lithologies at depth. On the other hand, due to the absence of magmatic zircons from the sill itself, the zircon dating was not suitable to date emplacement of the Arrikine sill.

5. Paleomagnetic dating

5.1 Sampling and analysis procedure

The sampling sites for paleomagnetism are located near the oued Arrikine (Fig. 2). 110 standard paleomagnetic samples, taken using a portable gasoline-powered drill and oriented with magnetic and sun compasses, were collected from the 12 sites (sites 50 to 61 on Fig. 2) in the gabbro (including one site in the weathered gray facies on the sill border and another one within a late dyke). 9 samples were chosen in one site (site 49 on the Figure 2) of Silurian host-rocks affected by contact metamorphism close to the roof of the sill. One to three specimens were cut from each core in order to have additional specimens for pilot studies and rock magnetic analysis. Prior to any demagnetization analysis, the specimens were stored in a zero field for at least one month, in order to reduce possible viscous components. The Natural Remanent Magnetization (NRM) of the specimens was measured using a JR5 spinner magnetometer (AGICO, Brno). Several pilot specimens from each site were subjected to a stepwise alternating field (AF) demagnetization up to 100 mT or thermal (TH) demagnetization up to 670°C in order to characterize the components of magnetization. Following combined demagnetization process, some other specimens were subjected to combined AF and TH treatments. The directions of the magnetization components were plotted on orthogonal vector plots (As and Zijderveld, 1958; Wilson and Everitt, 1963; Zijderveld, 1967) and the remaining vectors and vectorial differences of the magnetization on equal-area projections. The direction of the different components was computed using principal component analysis (Kirschvink, 1980). Fisher (1953) statistics was used to determine the mean directions.

334

335 ***5.2. Rock magnetism***

336 The NRM has a relatively high intensity in dark facies (mean 3.2 A/m) compared to
337 the weathered site close to the sill border (mean 2.7 10^{-2} A/m) and the late dyke (mean 5.3
338 10^{-2} A/m). AF demagnetization yields a relatively regular decrease of magnetization intensity.
339 For most samples, magnetization decrease during thermal demagnetization (Fig. 4) is
340 progressive (IZ647, IZ668) or steep above 400-450°C treatment up to about 530-560°C
341 (IZ654). These maximum blocking temperature values suggest the presence of Ti-poor
342 titanomagnetite as the principal mineral carrier. In few samples (Fig. 4), a strong increase of
343 the magnetization for about 400°C is followed by a sharp decrease around 450°C up to about
344 530-560°C (IZ718, IZ729). No increase appears during AF demagnetization of these samples,
345 for which complementary studies of the magnetic properties have to be performed and will be
346 the subject of an independent paper.

347 Thermomagnetic curves (low-field magnetic susceptibility as a function of
348 temperature) have been measured for representative samples by heating in air using CS2–3
349 oven and KLY3 Kappabridge (AGICO, Brno). For the gray weathered facies, during heating,
350 the partial cooling curves are often reversible with the heating ones (Fig. 5 - IZ696). In such
351 cases, irreversibility of the thermomagnetic curves appears only after heating at the highest
352 temperatures. During heating at temperatures higher than 400°C, a decrease of susceptibility
353 is observed, giving Curie temperature of about 550°C. This confirms that the principal
354 magnetic carrier is a Ti-poor titanomagnetite. However for some samples, a slight decrease
355 for temperatures higher than 580°C points out the presence of a small amount of hematite
356 besides the titanomagnetite (Fig. 5 - IZ696). In the dark facies, the sample thermomagnetic
357 curves are not reversible since 400 to 500°C heating, highlighting a relatively complicated
358 mineralogical alteration during heating at higher temperature (Fig. 6 IZ716).

359 Hysteresis loops were obtained for small cores (cylindrical samples of about 3 cm^3)
360 using a laboratory-made translation inductometer within an electromagnet capable of reaching
361 1.6 T. The loops show that the remanent coercive force determined from several
362 representative samples is low (around 30 mT) and that a partial saturation of the
363 magnetization is at least reached between approximately 0.2 to 0.4 T (IZ678, IZ725),
364 confirming the presence of a low coercivity component (like Ti-poor titanomagnetite). For
365 weathered gray facies, susceptibility is very low and almost linear hysteresis loops have been
366 obtained, indicating largely dominating effects of the paramagnetic minerals. For dark facies
367 (Fig. 6), a much higher susceptibility is associated with a clear dominance of ferrimagnetic

minerals. For these sites, Day plot (Day et al., 1977) indicates pseudo single-domain (PSD) grain size for the titanomagnetite (Fig. 6).

In conclusion, Ti-poor titanomagnetite is the main magnetic carrier in the non-weathered gabbro. It is also present in the weathered gray facies, but in much lower amount and associated with few hematite.

5.3. Paleomagnetic analyses

TH or AF or mixed AF-TH demagnetizations (Fig. 7) were performed on all samples. Very similar Characteristic Remanent Magnetization (ChRM B) data have been obtained from all methods, in addition to a viscous component A. During the demagnetization process, three different main kinds of evolution were observed for gabbro sites:

- The first type, obtained on half the samples, is illustrated by a single stable magnetic direction. Figures 7a, b and g show examples of this behavior obtained from an AF method (IZ659), thermal process (IZ 644) or mixed AF-TH (IZ660A). In this case, after elimination of the viscous component A, the analysis of the magnetization shows that the linear segments towards the origin on Zijderveld (1967) plots, define the ChRM B.
- The second type of behavior shows magnetic directions evolving first along a great circle (remagnetization circle), which indicates superimposition of the unblocking temperature (or unblocking fields) spectra for at least two remanent magnetization components. This evolution always reaches a ‘‘stable end point’’ direction yielding the ChRM B. This case is illustrated on the figures 7c and d for the AF method (IZ 709) and the thermal method (IZ 739). Here also, similar results are obtained by the two method of demagnetization. The secondary component at the origin of the variation along the great circles cannot be properly identified. It could correspond to a Cenozoic overprint (Henry et al., 2004; see also for example Hargraves et al., 1987), but other origins cannot be rejected by lack of constraints.
- The third case (Figs. 7e, f) displays similar variation than the first case, except that, during the thermal treatment, a component, with the same direction as the main magnetization but with opposite polarity, appears at c. 400°C and progressively disappears at higher temperature (from c 500°C), yielding a well-defined ChRM magnetization. During AF demagnetization, this intermediate component of opposite polarity is not present. The final ChRM directions obtained for both demagnetization processes are the same. This additional component is therefore related to a mineralogical alteration due to heating. These samples will be the subject of a complementary analysis about magnetic properties.

The ChRM B obtained from samples with these three behaviors was isolated between 200 and 500 °C for the lowest temperatures and 400–560°C for the highest ones (thermal process), and between 10-70 mT for the lowest blocking field and 60 and 102 mT for the highest ones (AF demagnetization).

Results from the sites sampled in weathered facies on the sill border (14 samples) and within a late dyke (12 samples) are mostly not reliable. The obtained results from all the other samples are homogeneous (Table 4). The mean direction of this ChRM B computed from 84 specimens (from 12 sites) has the following directions: D = 355.4°, I = -38.4°, k = 38, α_{95} = 2.5° and D = 350.7°, I = -38.6°, k = 38, α_{95} = 2.5°, before and after dip correction, respectively (Table 4 – Fig. 8). This result is similar to that obtained from the mean direction of the 10 sites (two sites with less than 3 ChRMs being not considered): D = 355.5°, I = -38.8°, k =86, α_{95} = 5.2° and D = 350.6°, I = -38.9°, k = 86, α_{95} = 5.2°, before and after dip correction, respectively (Fig. 8).

The paleomagnetic data obtained from the site of Silurian host-rocks affected by contact metamorphism have similar characteristics with neighboring ChRM orientation (N=9 samples, D = 358.6°, I = -42.8°, k =402, α_{95} = 2.6° and D = 349.5°, I = -41.7°, k = 402, α_{95} = 2.6°, before and after dip correction, respectively) but with lower magnetization intensity. Other sites, taken in the Ordovician and Silurian rocks far from the sill (sites 43 to 48 on Fig. 2), yield only weak Cenozoic remagnetization of normal and reversed polarity (see Henry et al., 2004), totally overprinting any possible previous earlier magnetization. That is then not the case for the site affected by contact metamorphism. The samples from this site carried a much more stable magnetization than the other sites. That is attributed to an effect of the contact metamorphism generated by the sill. This kind of positive contact test strongly argues for a primary magnetization of the gabbro.

The corresponding paleomagnetic pole determined from the sill data is defined by λ = 43.6°S, ϕ = 17.0°E, K = 88 and A_{95} = 4.7° and λ = 42.8°S, ϕ = 22.9°E, K = 88 and A_{95} = 4.7°, before and after bedding correction, respectively.

5.4 Paleomagnetic dating of the Arrikine sill

A gabbro magnetization age younger than the post-Cretaceous tilting of the formations is unrealistic when comparing the Arrikine poles with the known Apparent Polar Wander Path - APWP - (Fig. 9) and data can only be used after applying a bedding correction. The so corrected Arrikine pole (Fig. 9) corresponds to the Gondwana APWP segment for the 400 Ma period of Derder et al., 2006, Amenna et al., 2014 and Henry et al., 2015 and to that of

Torsvik et al., 2012 (overlapping of confidence zones) for the 410 Ma mean pole. In the latter, the uncertainty on the paleomagnetic mean pole age is not taken into account while it corresponds to a single pole (Aïr intrusives, Hargraves et al., 1987), which can explain the difference existing with the former one. Indeed, integration of such uncertainties in the first APWP adds a weighted effect for poles having a large age uncertainty and thus covering several windows in time, smoothing the curve. This is particularly critical for periods affected by strong changes of the APWP drift such as the 400-410 Ma period (Fig. 9). Geologically, the Arrikine sill is post-Silurian and pre-Cretaceous. The Arrikine pole is very far from all mean paleopoles from Middle Devonian to Present times, especially for Carboniferous times. It is also far from Silurian mean paleopoles (Fig. 9). By contrast, the Arrikine pole is consistent with Early Devonian poles of Gondwana: Mt. Leyshon Devonian dykes in Australia (Clark, 1996), Snowy River Volcanics in Australia (Schmidt et al., 1987), Herrada Member, Sierra Grande in Argentina (Rapalini and Vilas, 1991) and Aïr alkaline ring-complexes in Niger (Hargraves et al., 1987). In particular, the coincidence of the Arrikine pole with this last pole ($\lambda = 43.4°S$, $\phi = 8.6°E$, $K = 50$ and $A_{95} = 6.2°$) is remarkable. The angular difference between these paleomagnetic poles (10.7°) is of the order of what can be ascribed to the secular variation. In both the Arrikine sill and the Aïr alkaline ring-complexes, the paleomagnetic directions have the same single polarity. So the Aïr ring-complex age of 407±8 Ma (Moreau et al., 1994) can be considered as a good approximation of the age of the Arrikine sill, which can be fixed to the 400-415 Ma age interval, i.e. at the base of the Emsian, from mid-Lochkovian to mid-Emsian (Cohen et al., 2013), thus globally Lower Devonian.

The loop of the Gondwana APWP between the Late Ordovician (pole 450 Ma) and Late Devonian (370 Ma) was not generally deemed as very reliable. The Aïr and Arrikine coherent mean is "unique" and supports the existence of this loop that has to be considered for the paleocontinental reconstructions for this period.

6. Geochemistry

Only one analysis (sample AF-ALG/Dj-Site58 from site 58 – Fig. 2) is available and listed in Table 5. However, its geochemical signature (Fig. 10) is sufficiently diagnostic to allow a proper geochemical characterization of the Arrikine sill and to deduce constrained conclusions about its origin. All oxides are considered in column a* as deduced from the geochemical analysis by ICP and in column b* are recalculated to 100% on an anhydrous basis. Oxide % are always wt. %, unless otherwise stated. The Arrikine sill is a fine-grained

gabbro but (see below) its chemistry is similar to intraplate alkali basaltic rocks in continental flood basalt (CFB) and ocean island basalt (OIB) provinces. So, in order to make the comparison more efficient, geochemical diagrams dedicated to volcanic rocks and volcanic nomenclature are applied here, which is justified by the subvolcanic character of the sill and by the difficulty of counting a mode on this kind of rock.

The Arrikine gabbro having 45.99% SiO_2 and 5.79% Na_2O+K_2O, on an anhydrous basis, belongs to the alkali series, being an alkali gabbro. It has the composition of a trachybasalt (Le Bas et al. 1986), more precisely of an hawaiite (wt%Na_2O-2 > wt%K_2O), i.e. a sodic trachybasalt (Le Maitre et al., 2002). The depleted MgO content (4.1%) corresponds to typical hawaiite (3 - 5.5 % MgO; MacDonald and Katsura, 1964) as is the absence of chromite (Cr: 3 ppm; Ni: 39 ppm), a characteristic of hawaiite (Cr: 5-150 ppm; Ni: 5-80 ppm; Nelson and Carmichael, 1984 and references therein), in agreement with the differentiated character of hawaiites. Immobile trace elements confirm that the Arrikine gabbro has the composition of an alkali basalt with Nb/Y= 0.85 and Zr/TiO_2*0.0001= 0.0064 (diagram not shown; Winchester and Floyd, 1977). Low concentration of Ni, Cr and absence of positive Eu anomaly do not point to a significative cumulative component. Even the very low Cr content in Arrikine gabbro points to a differentiated character.

In addition, with TiO_2 = 5.01%, the Arrikine gabbro belongs to the high-Ti series (TiO_2 >2%); it has the composition a high-Ti alkali basalt. CIPW norm points to 60% plagioclase (An30), 11% K-feldspar, 9% pyroxene, 6% olivine, 2% apatite and 11% Fe-Ti oxides (Table 5) in rough agreement with the petrography except that the plagioclase is acid (actually Labrador) and the absence of biotite, not computed in the norm. This norm is in agreement with a composition of a high-Ti hawaiite. The important difference in the An content of the plagioclase can be ascribed to the late “aplitic” phase determined by the microprobe measurements to be acid oligoclase (An13-17). The An30 value determined by the norm suggests that this aplitic phase was quite pervasive at least in the analyzed sample. This implies that concerned elements (i.e. K, Ba but also Rb, Sr) must be used with caution when the original magma is concerned as well as the K-Ar age for which we have calculated (method based on an initial age of 410 Ma given by paleomagnetic considerations and the rejuvenated result at 326 Ma) a K enrichment of up to 20 %.

The contemporaneous (407 ± 8 Ma; Moreau et al., 1994) large province of alkaline ring-complexes of Aïr bears also high-Ti gabbros, especially the large Ofoud ring-complex where they are associated with numerous layers and/or lenses of titanomagnetite up to 10 m thick (Karche and Moreau, 1978) and the smaller Abontorok ring-complex, associated with

503 massive anorthosites (Brown et al., 1989). These gabbros are of uniform grain size (2-7 mm)
504 and massive in texture and titanomagnetite and ilmenite can make up as much as 10 percent
505 of the rock (Hush and Moreau, 1982). The Aïr ring-complex province is intrusive along the
506 western boundary of the Saharan metacraton (Liégeois et al., 1994, 2013) as a consequence of
507 its reactivation during early Devonian (Moreau et al., 1994). The Arrikine gabbro is compared
508 to the available analysis from Abontorok ring complex (Brown et al., 1989) and to several
509 intraplate continental high-Ti alkali basalt or gabbro provinces: the Trias rift-related from SW
510 China, similar to the high-Ti basalts from the Emeishan LIP (Zhang et al., 2013), the
511 Ordovician Suordakh and Cambrian Kharaulakh mafic rocks from Siberia (Khudoley et al.,
512 2013) or the 1.5 Ga Yangtse mafic province (Fan et al., 2013). We added also for comparison
513 the intraplate high-Ti potassic basalts from the Virunga (Rogers et al., 1998).

514 When compared to these high-Ti alkali basalts from different settings and different
515 ages, the Arrikine gabbro has globally a similar pattern (Fig. 10). Compared to Mauna Loa
516 volcano in Hawaii (Wanless et al., 2006), the Arrikine gabbro displays a subparallel REE
517 pattern, being slightly more enriched, especially in LREE (Fig. 3a). Similarly, its pattern in
518 the spidergram (Fig. 10b) is parallel, only very slightly enriched in HFSE, more enriched in
519 LILE especially in Ba. High-Ti basalts have a largely preponderant mantle origin by contrast
520 to low-Ti basalts (e.g. Deckart et al., 2005), explaining similar compositions in the oceans and
521 in the continents. This characteristic renders, however, this kind of magmas relatively rare
522 within the continents, which is an important fingerprint of the Arrikine sill. The spatially close
523 Aïr high-Ti gabbros (Abontorok ring complex; Brown et al., 1989) display REE patterns close
524 to that of Arrikine (Fig. 10a) except for Eu, probably due to a plagioclase cumulative pattern
525 (Aïr ring-complexes comprise massive anorthosites - Brown et al., 1989; Demaiffe et al.,
526 1991). Abontorok spidergrams are also close to that of Arrikine, the latter being on the most
527 enriched side. This can be related to its low Cr content suggesting a differentiated character,
528 the differentiation being able to concentrate incompatible elements. However, in the Arrikine
529 gabbro Rb, Ba and K appear particularly enriched; these enrichments can be related to the
530 presence of the late metasomatic aplitic phase (See K-Ar section; Table 5) probably favored
531 by the sedimentary environment. This is particularly visible when compared with the
532 Suordakh high-Ti basalt from Siberia (Khudoley et al., 2013) in a primitive mantle-
533 normalized graph (Fig. 11): the Arrikine basalt is very similar to the Suordakh basalts but
534 with concentrations in K as high as the richer Suordakh basalts and with Ba contents much
535 higher than any Suordakh basalts. This indicates that the K, Rb and Ba concentrations in the
536 pristine Arrikine gabbro were probably lower than that currently observed. By opposition, the

other elements (HFSE, Th) can be considered as pristine, being not mobilized by an aplitic fluid.

If the Arrikine gabbro composition is similar to the intraplate alkaline continental high-Ti alkali basalt or gabbro provinces, it is distinct from the intraplate high-Ti potassic basalts from the Virunga (Rogers et al., 1998), except for Ba. By opposition to the latter, the sources of the formers are considered to be a more or less enriched asthenospheric source with very low lithospheric participation, similarly to Hawaii volcanoes but in a continental setting. The similarity of the geochemistry of the Arrikine sill with the lower Devonian Aïr magmatism concurs to support the lower Devonian age determined in the paleomagnetic section.

Based on the silica content, a simple calculation leads to an estimated liquidus temperature of 1280°C. When considering the experimental work of Botcharnikov et al. (2008) determining a liquid line of descent for ferro-basalts, the Arrikine concentrations in SiO_2, MgO, TiO_2, K_2O, Na_2O, Al_2O_3, FeO, CaO point all to a temperature of c. 1080°C, which is the temperature where the maximum concentration in FeO and TiO_2 is attained. This is true when considering nearly anhydrous magmas, which is the case of Arrikine (0.2% H_2O, Table 5). Considering the temperature of the mantle partial melting at 1280°C and the crystallization of the Arrikine sill at 1080°C seems reasonable. This is indeed the temperature range observed in experimentation concerning Fe-rich basalts (Chevrel et al., 2014). The calculated viscosity at liquidus temperature is very low (0.17 Pas), as it is the case for Fe-rich basalts whose viscosity is less than 1 Pas (Chevrel et al., 2014). In a 3 m-width dyke, a magma rise speed higher than 10 m/s can be proposed, a speed that limits fractional crystallization and interaction with country-rocks during ascent (Chevrel et al., 2014). This implies that the differentiation that affected the Arrikine magma (low Cr contents) occurred at depth.

Most of these provinces are considered to be or having been fed by a mantle plume. Notwithstanding the fact that the existence of mantle plumes is currently challenged (e.g. Foulger and Hamilton, 2014), there is no one argument for a plume origin in the case of the Arrikine sill: very small magmatic volume, no swell, no rift, no magmatic track, even if a similar asthenospheric mantle source can be inferred for the Arrikine sill. The proposed alternative will be discussed below in the geodynamic section.

7. Emplacement and reactivation of the Arrikine sill: why there and why at these times?

7.1 Regional considerations

7.1.1. The time of emplacement, the Lower Devonian

During the Pan-African orogeny and the Phanerozoic, the Murzuq craton played an important role as a rheologically rigid body. Magmatism and compressive (Pan-African) or extensional (Phanerozoic) tectonics occurred around it, and the Murzuq basin developed as an intracontinental sag basin in a similar way as Al Kufra and Chad basins (Heine et al., 2008). Formation of the Murzuq basin did not require accommodation of tectonic subsidence through faulting and rifting but resulted from the negative buoyancy caused by thick cratonic lithosphere (Ritzmann and Faleide, 2009). As a consequence, the Murzuq craton is devoid of magmatism except along its metacratonic boundaries where Cenozoic volcanic fields are particularly present all around it (Fezaa et al., 2010; Liégeois et al., 2013). Indeed, the West African Cenozoic volcanism is attributed to tectonic reactivations induced by the Europe-Africa convergence (Liégeois et al., 2005; Beccaluva et al., 2007; Lustrino et al., 2012; Radivojević et al., 2015). These reactivations, even induced by the rather low stress propagating in remote intracontinental regions, must affect the whole lithospheric thickness allowing for small mantle melt volumes to reach the surface. This is the case of the mega-shear zones within metacratonic areas that are rigid but fractured (Liégeois et al., 2003, 2005, 2013; Bardintzeff et al., 2011) through vertical planar delamination as recently evidenced by magnetotelluric studies in Hoggar (Bouzid et al., 2015).

The Arrikine sill is lower Devonian in age and intruded Silurian sediments. It can be correlated with Paleozoic dolerites in Niger (Fig. 1B), which are also intrusive within Silurian sediments, suggesting a regional event along the southwestern border of the Murzuq basin, even if limited in volume.

By opposition, no direct evidence of magmatism, even as detrital pebbles, were described within the sedimentary Devonian formations of the Murzuq basin (Bellini and Massa, 1980). This fact is tentatively related to the so-called Caledonian event (base of the Devonian) that prevented the deposition of lower Devonian sediments (Ghienne et al., 2013). This “Caledonian” event” was marked in the Murzuq basin by large scale uplifts and secondary highs roughly oriented SSE–NNW in SW Libya, i.e. parallel to the Pan-African major shear zones in the Djanet and Edembo terranes (Davidson et al., 2000; Ghienne et al., 2013) constituting the western metacratonic boundary of the Murzuq craton (Fezaa et al., 2010).

This means that the Arrikine sill intruded during a period of reactivations of the mega-shear zones of the region, known to be former terrane boundaries and as such of lithospheric scale (Fezaa et al., 2010). The Aïr ring complex province also resulted from the reactivation of a major shear zone, the Raghane shear zone (Moreau et al., 1994), which corresponds to the western boundary of the Saharan metacraton (Liégeois et al., 1994; Abdelsalam et al., 2002). The shift from the rapid vertical ascent along the mega-shear zone of the low-viscosity Arrikine magma to the widespread horizontal sill development can be tentatively attributed to the characteristics of the Silurian Acacus formation. The latter is a massive level (about 100 m thick) overlying lagunal deposits that include gypsum-rich beds (Freulon, 1964). We thus suggest that the Arrikine magma intruded within evaporitic-rich facies, which, at the contact with the high temperature magma, became much more easily deformable and moreover released water due to gypsum transformation, largely blocking the magma ascent. However, looking at the age of the magmatism and at the stratigraphic series, the Arrikine sill should have intruded the cover at shallow depth (of the order of less than 300 m), in agreement with the moderate size (PSD) of the magnetite grains. These renders the presence of Arrikine aerial products likely but in that case it is likely that they were eroded and transported far away by the large fluvial system that developed at this period in the Murzuq basin (Ghienne et al., 2013) as it was the case for most of the Lower Devonian deposits in the Murzuq basin (Davidson et al., 2000).

This kind of emplacement would be favorable to suggest a link between the Arrikine magmatism and the magmatic rocks proposed to be at the origin of sand injections in the Murzuq area (Fig. 1A; Moreau et al., 2012). Indeed, these peculiar structures occur in the Silurian sediments around the Murzuq basin in a similar manner as the Arrikine sill and are considered as Devonian in age. These sand injections would be the result of the combined effects of tectonic uplift, igneous intrusions in the sand-rich Cambrian-Ordovician sediments and overpressures generated by the paleo-relief existing below the Silurian strata (Moreau et al., 2012). The Arrikine sill would correspond to the magma that intruded the Silurian sediments, lower Devonian sediments having not deposited in the area due to uplift. Let us remark that the three known occurrences of sand injections (Mt Telout, In-Ezzane to the west and El Meherschema to the east; Fig. 1A) are also located around the Murzuq craton, within its metacratonic margin, the Tibesti area being the equivalent of the Djanet and Edembo terranes from Eastern Hoggar (Fezaa et al., 2010).

7.1.2. The time of rejuvenation, the Mid-Carboniferous

The K-Ar method has given an age of 325.6 ± 7.7 Ma that we consider as close to that of a rejuvenation event during the Serpukhovian, i.e. from uppermost Visean to upper Bashkirian when taking into account the error bracket-attributed to aplitic fluid percolation. Such an age is also that of the erasure of the primary magnetization in the older sedimentary rocks of the Saharan platform (Henry et al., 2004). It corresponds thus to the second main tectonic event in the area. This Mid-Carboniferous compression event led to the major so-called Hercynian unconformity that affected the upper part of the Paleozoic sequence in the Murzuq Basin but whose initial phases started during middle Carboniferous (Bellini and Massa, 1980), or at the Visean-Serpukhovian boundary (Fröhlich et al., 2010 and references therein). This event was responsible for the uplift of the Tiririne High (NW Murzuq basin) at the end of the Visean, removing the Assedjefar-Marar (Lower Carboniferous) sequence (Echikh and Sola, 2000). It began with transpressional movements along a series of NNE-SSW trending wrench faults (parallel to the Murzuq craton boundary), producing a NE-SW en echelon pattern of folds on the Tiririne High (Echikh and Sola, 2000). At the scale of the Murzuq basin, the last marine deposits are of Moscovian age (e.g. Massa et al., 1988; Amenna et al., 2014) and the upper Carboniferous is nearly entirely lacking (due to uplift or to erosion) and only some red lacustrine mudstone (e.g. upper Carboniferous Tiguentourine Formation) can be rarely found (Davidson et al., 2000).

Such a major compressive event, with transpressional movements and various uplifts at the regional scale is favorable for fluid movements, able to reset the K-Ar geochronometer that in turn is able to date it. A Serpukhovian reactivation ("Hercynian") occurred at the same place as the early Devonian ("Caledonian") reactivation. This indicates that emplacement of the Arrikine sill was related to the lithospheric character of the mega-shear zones of the region (Fezaa et al., 2010). This implies that these intraplate reactivations are quite important and must be considered.

7.2 Global considerations

For a long time, the use of the "Caledonian" and "Hercynian" expressions was suggested for the intraplate intense tectonic reactivations that occurred around the Murzuq craton. Causes must be found in events that occurred at the plate margins at these periods. In addition to tectonic reactivations, volcanism may be generated by adiabatic pressure release of uprising asthenosphere in response to stress resulting from far field collisions such as, for the West African Cenozoic volcanism, the Africa-Europe collision (Liégeois et al., 2005). Indeed,

these “Caledonian” and "Hercynian" effects are known all over the Saharan platform, to the north of Hoggar (Haddoum et al., 2001; Galeazzi et al., 2010), around the West African craton (Michard et al., 2008) or within the Algerian petroleum basins (Galeazzi et al., 2010) and in the whole Northern Africa (Guiraud et al., 2005). The Alpine reactivation is generally superimposed on the Hercynian reactivated structures (Smith et al., 2006, Derder et al., 2009). These “Caledonian” and "Hercynian" tectonic events are also recorded at the regional scale by detrital zircons in the Murzuq basin (Morton et al., 2011).

The Arrikine sill emplacement, as well as that of the Aïr ring-complex province (Moreau et al., 1994) at c. 410 Ma, occurred during a continental breakup, when the Hun terranes separated from the northern Gondwana margin (Stampfli and Borel, 2002, Blackey, 2008 and references therein). Such a geodynamical environment is favorable to generate intraplate tectonics and magmatism as it was the case, for West Africa, during the continental breakup. This led to the Atlantic ocean opening that generated the Central Atlantic Magmatic Province (CAMP; Marzoli et al., 1999), which extends in West Africa (e.g. Chabou et al., 2007, 2010), SW Europe (Callegaro et al., 2013) and even Sicily (Cirrincione et al., 2014), and East America, including Bolivia (Bertrand et al., 2014). This province, even tholeiitic, comprises abundant high-Ti basalts related to an asthenospheric mantle source (Deckart et al., 2005). We thus suggest that the Arrikine sill, and associated magmatism, emplaced due to this continental breakup that also generated the Caledonian unconformity.

The mid-Carboniferous reactivation with an age at 325.6 ± 7.7 Ma as determined by the K-Ar method is easily related to the late Variscan episode that resulted from the collision between Gondwana, especially NW Africa, and southern Europe from 330 Ma to early Permian (Schulmann et al., 2014). The fact that this important event generated no magmas (except the aplitic metasomatism) can be related to the transpressive character of this reactivation, unable to allow magmas to rise if no major horizontal movements occurred, as it is the case in an intraplate setting.

To sum up, we propose that the Arrikine sill was emplaced along a major lithospheric weakness zone, the margin of the Murzuq craton during the Gondwana-Hun continental breakup. Similarly, the reactivation of the major Raghane shear zone bordering the Saharan metacraton that allowed the emplacement of the Aïr ring complex province (Moreau et al., 1994), can be attributed to this continental break-up. This lithosphere weakness zone was reactivated during the late Variscan orogeny that involved Gondwana. These two events correspond to the two major unconformities with important sedimentary hiatus known in the region, the so-called Caledonian and Hercynian unconformities.

8. Conclusions

The newly discovered Arrikine sill is a large magmatic object (pyroxene-rich gabbro) of Lower Devonian age emplaced in Silurian sediments, rather unexpected in far-east Hoggar. Although emplaced in an intraplate environment, its datation was not straightforward: all zircons are older than the country rocks and are thus inherited (most zircons are at c. 2030 Ma with additional ages at c. 2700 Ma and in the 766-598 Ma age range) and its rejuvenated K-Ar age of 325.6 ± 7.7 Ma relates to a remobilization event due to a K-rich aplitic fluid that reset the isotopic system and that is recorded by secondary minerals (K-feldspar, acid plagioclase, quartz). By contrast, the paleomagnetic pole is reliable and allows dating of the Arrikine sill emplacement in the 400-415 Ma age interval (mid-Lochkhovian-mid-Emsian).

Geochemically, the Arrikine gabbro has the composition of a high-Ti alkali basalt, actually a high-Ti hawaiite (sodic trachybasalt), with 46% SiO_2, 4% MgO, $\%Na_2O-2>\%K_2O$, absence of chromite and 5% TiO_2. As a whole, this chemistry is close to that of the Mauna Loa volcano in Hawaii (Wanless et al., 2006), in agreement with an enriched mantle origin needed for such a high-Ti/low-Si composition. This peculiar chemistry is similar to several intraplate continental provinces such as the Trias rift-related from SW China, the high-Ti basalts from the Emeishan LIP (Zhang et al., 2013), the Ordovician Suordakh and Cambrian Kharaulakh mafic rocks from Siberia (Khudoley et al., 2013) or the 1.5 Ga Yangtse mafic province (Fan et al., 2013). It is also similar to some lithologies belonging to the lower Devonian Aïr ring complexes province in Niger, such as the Abontorok ring complex (Brown et al., 1989). The peculiarity of these compositions supports so a lower Devonian age for the Arrikine sill, as is proposed in the paleomagnetic section. The Arrikine gabbro composition points to a liquidus temperature of 1280°C and a temperature of 1080°C for the magma when it crystallized close to the surface.

Geodynamically, the Arrikine sill emplaced in Silurian sediments belonging to the western boundary of the Murzuq craton, actually its metacratonic margin (Fezaa et al., 2010; Liégeois et al., 2013). Its emplacement is related to the reactivation of this metacratonic margin due to a low stress that propagated in this remote intracontinental region. This was a consequence of "Caledonian" events that also generated in the area the so-called Caledonian unconformity, witness of the absence of lower Devonian sediment deposition (e.g. Ghienne et al., 2013). A link with the magmatic rocks at the origin of the sand injections at the Murzuq craton margins (Moreau et al., 2012) is suggested. The Aïr ring complexes were emplaced at

the same period, also along a major lithospheric discontinuity, the Raghane shear zone (Moreau et al., 1994), which is the western boundary of the Saharan metacraton (Abdelsalam et al., 2002).

The Mid-Carboniferous rejuvenation dated by the K-Ar age (325.6 ± 7.7 Ma) and marked by a aplitic fluid phase can be correlated with the erasure of the primary magnetization in the older sedimentary rocks of the Saharan platform (Henry et al., 2004). It corresponds to the second main Phanerozoic tectonic event in the area marked by the so-called Hercynian unconformity, responsible for important transpressive vertical movements such as the uplift of the Tiririne High (NW Murzuq basin).

Emplacement (c. 410 Ma) and rejuvenation (c. 326 Ma) of the Arrikine sill are thus attributed to intense tectonic reactivations that occurred around the Murzuq craton, able to generate magmas of mantle origin through adiabatic pressure release of uprising asthenosphere along mega-shear zones. The effects of these two events being known all over the Saharan platform, it is concluded that they resulted from major events that occurred at plate boundaries. We suggest that the extensional event in the Arrikine area at 410 Ma is linked to the continental breakup when the Hun terranes separated from the northern Gondwana margin (Stampfli and Borel, 2002, Blackey, 2008 and references therein) and, that the compressional event at c. 325 Ma reflects the far-field effects of the collision between Africa (belonging to Gondwana) and southern Europe (Schulmann et al., 2014).

Acknowledgements

This project was supported by the Algerian-French PICS cooperation program "Architecture lithosphérique et dynamique du manteau sous le Hoggar". We are very grateful to the civil and military authorities at Djanet and to the "Office du Parc National du Tassili" - OPNT (now "Office National du Parc Culturel du Tassili N'ajjer" - ONPCTA) for help during the field work. Whole-rock analyses were measured on the Horiba-Jobin-Yvon Ultima 2 ICP-AES at the IUEM, Pôle de Spectrométrie Océan, Brest, France. Céline Liorzou is thanked for her essential geochemical contribution. Microprobe analyses were performed using the Ouest Microprobe located at Brest. Jessica Langlade is thanked for the feldspars analyses. We are very grateful to Rob Van der Voo for his detailed and constructive review.

References

Abdelsalam M., Liégeois J.P., Stern R.J., 2002. The Saharan metacraton. Journal of African Earth Sciences, 34, 119-136

Amenna M., Derder, M.E.M., Henry, B., Maouche, S., Bayou, B., Bouabdallah, H., Ayache, M., Bediaf, M., 2014. Improved Moscovian part of the Gondwana APWP for paleocontinental reconstructions, obtained from a first paleomagnetic pole, age-constrained by a fold test, from In Ezzane area in the Murzuq basin (Algeria, stable Africa). Journal of African Earth Sciences, 99, 342-352. doi.org/10.1016/j.jafrearsci.2013.12.006.

As J.A., Zijderveld J.D.A., 1958. Magnetic cleaning of rocks in paleomagnetic research. Geophs. J. R. astr. Soc., 1, 308-319.

Bardintzeff, J.-M., Deniel, C., Guillou, H., Platevoet, B., Telouk, P., Oun, K.M., 2011. Miocene to recent alkaline volcanism between Al Haruj and Wawan Namous (southern Libya). International Journal of Earth Sciences. 101, 1047–1063.

Beccaluva, L., Azzouni-Sekkal, A., Benhallou, A., Bianchini, G., Ellam, R.M., Marzola, M., Siena, F., Stuart, F.M., 2007. Intracratonic asthenosperic upwelling and lithosphere rejuvenation beneath the Hoggar swell (Algeria): evidence from HIMU metasomatised lherzolite mantle xenoliths. Earth Planet. Sci. Lett. 260, 482–494.

Bellini, E., Massa, D., 1980. Stratigraphic contribution to the Palaeozoic of Southern basins of Libya. In: Salem, M.J., Busrewil, M.T. (Eds.), Geology of Libya (I). Academic Press., London, pp. 2-56.

Bellon, H., Quoc Buu, N., Chaumont, J., Philippet, J.C., 1981. Implantation ionique d'argon dans une cible support : application au traçage isotopique de l'argon contenu dans les minéraux et les roches. Comptes Rendus de l'Académie des Sciences de Paris II, 292, 977-980.

Bertrand, H., Fornari, M., Marzoli, A., García-Duarte, R., Sempere, T., 2014. The Central Atlantic Magmatic Province extends into Bolivia. Lithos 188, 33–43.

Black, R., Jaujou, M. and Pellaton, C., 1967. Notice explicative sur la carte géologique de l'Air à l'échelle du l/500 000ème. Dir. Mines Geol., Niamey.

Blackey, R.C., 2008. Gondwana paleogeography from assembly to breakup — A 500 m.y. odyssey", in Fielding, C.R., Frank, T.D., and Isbell, J.L., eds., Resolving the Late Paleozoic Ice Age in Time and Space. Geological Society of America Special Paper 441, 1-28.

Boehnke, P., Watson, E.B., Trail, D., Harrison, T.M., Schmitt, A.K., 2013. Zircon saturation re-revisited. Chemical Geology, 351, 324–334

Bonin, B., Ouabadi, A., Liégeois, J.P., Bruguier, O., Passchier, C., Guillou, H., Abdallah, N., Fezaa, N., Laouar, R., Boissonnas, J., 2011. Possible impact craters within the In Ezzane Quaternary volcanic province, Eastern Hoggar, Algeria. The Second Arab Impact Cratering and Astrogeology Conference (Aicac II), Casablanca, Morocco.

Bosch, D., Bruguier, O., Pidgeon, R.T, 1996. Evolution of an Archean Metamorphic Belt: a conventional and SHRIMP U-Pb study of accessory minerals from the Jimperding Metamorphic Belt, Yilgarn Craton, West Australia. Journal of Geology, 104, 695-711.

Bosch, D., Garrido, C.J., Bruguier, O., Dhuime, B., Bodinier, J.L., Padron-Navarta, J.A., Galland, B., 2011. Building an island-arc crustal section : Time constraints from a LA-ICP-MS zircon study. Earth Planetary Science Letters, 309, 268-279.

Botcharnikov, R.E., Almeev, R.R., Koepke, J., Holtz, F., 2008. Phase relations and liquid lines of descent in hydrous ferrobasalt - Implications for the Skaergaard Intrusion and Columbia River Flood Basalts. Journal of Petrology, 49, 1687-1727.

Bouzid, A., Bayou, B., Liégeois, J.-P., Bourouis, S., Bougchiche, S.S., Bendekken, A., Abtout, A., Boukhlouf, W., and Ouabadi, A., 2015. Lithospheric structure of the Atakor metacratonic volcanic swell (Hoggar, Tuareg Shield, southern Algeria): Electrical constraints from magnetotelluric data. In Foulger, G.R., Lustrino, M., and

King, S.D., eds., The Interdisciplinary Earth: A Volume in Honor of Don L. Anderson: Geological Society of America Special Paper 514, 239-255.

Callegaro, S., Rapaille, R., Marzoli, A., Bertrand, H., Chiaradia, M., Reisberg, L., Bellieni, G., Martins, L., Madeira, J., Mata, J., Youbi, N., De Min, A., Azevedo, M.R., Bensalah, M.K., 2014. Enriched mantle source for the Central Atlantic magmatic province: new supporting evidence from Southwestern Europe. Lithos, 188, 15-32.

Chabou, M., C., Sebai, A., Féraud, G., Bertrand, H., 2007. Datation 40Ar/39Ar de la province magmatique de l'Atlantique central dans le Sud-Ouest algérien. C. R. Geoscience, 339, 970–978.

Chabou, M.C., Bertrand, H., Sebai, A., 2010. Geochemistry of the Central Atlantic Magmatic Province (CAMP) in south-western Algeria. Journal of African Earth Sciences 58, 211–219

Chevrel, M.O., Baratoux, D., Hess, K.-U., Dingwell, D.B., 2014. Viscous flow behavior of tholeiitic and alkaline Fe-rich Martian basalts. Geochimica et Cosmochimica Acta 124, 348-365

Cirrincione, R., Fiannacca, P., Lustrino, M., Romano, V., Tranchina, A., 2014. Late Triassic tholeiitic magmatisminWestern Sicily: A possible extension of the Central Atlantic Magmatic Province (CAMP) in the Central Mediterranean area? Lithos, 188, 60–71.

Clark, D.A., 1996. Palaeomagnetism of the Mount Leyshon intrusive complex, the Tuckers igneous complex and the Ravenwood Batholith. CSIRO Australian Exploration Mining Report, 318R.

Cohen, K.M., Finney, S.C., Gibbard, P.L., Fan, J.X., 2013. The ICS international chronostratigraphic chart. Episodes, 36, 199-204.

Cox, A., Dalrymple, G.B., 1967. Statistical analysis of geomagnetic reversal data and the precision of potassium-argon dating. Journal of Geophysical Research, 72, 2603-2614.

Davidson, L., Beswetherick, S., Craig, J., Eales,M., Fisher, A., Himmali, A., Jho, J., Mejrab, B., Smart, J., 2000. The structure, stratigraphy and petroleum geology of the Murzuq Basin, southwest Libya. In: Geological Exploration in Murzuq Basin (M.A. Sola and D. Worsley, editors), Elsevier, Amsterdam, 295-320

Day, R., Fuller, M., Schmidt, V.A., 1977. Hysteresis properties of titanomagnetites: grain size and compositional dependence. Physics of the Earth and Planetary Interiors 13: 260-267

Deckart, K., Bertrand, H., Liégeois, J.P., 2005. Geochemistry and Sr, Nd, Pb isotopic composition of the Central Atlantic Magmatic Province (CAMP) in Guyana and Guinea. Lithos, 82, 282-314

Derder, M.E.M., Henry, B., Bayou, B., Ouabadi, A., Bellon, H., Djellit, H., Khaldi, A., Amenna, M., Baziz, K., Hemmi, A., Guemache, M.A., 2006. New African Lower Carboniferous paleomagnetic pole from intrusive rocks of the Tin Serririne basin (Southern border of the Hoggar, Algeria). Tectonophysics, 418, 189–203.

Derder, M.E.M., Henry, B., Amenna, M., Bayou, B., Djellit, H Guemache, M.A., Hemmi, A.. 2009. New structural implications for central Sahara (Algeria) from revisited Upper Carboniferous "Hassi Bachir" formation: Paleomagnetic constraints. Tectonophysics, 463, 69-76, doi:10.1016/j.tecto.2008.09.012.

Djellit, H., Bellon, H., Ouabadi, A., Derder, M.E.M., Henry, B., Bayou, B., Khaldi, A., Baziz, K., Merahi, M.K., 2006. Age $^{40}K/^{40}Ar$, Carbonifère inférieur, du magmatisme basique filonien du synclinal paléozoïque de Tin Serririne, sud-est Hoggar (Algérie). Comptes Rendus Geosciences. 338, 624-631.

Domeier, M., Van der Voo, R., Torsvik, T.H., 2012. Paleomagnetism and Pangea: The road to reconciliation. Tectonophysics, 514-517, 14-43.

868 Echikh, K., Sola, M.A., 2000. Geology and Hydrocarbon Occurrences in the Murzuq Basin,
869 SW Libya. In: Geological Exploration in Murzuq Basin (M.A. Sola and D. Worsley,
870 editors), Elsevier, Amsterdam, 175-222.
871 Fan, H.-P., Zhu, W.-G., Li, Z.-X., Zhong, H., Bai, Z.J., He, D.F., Chen, C.-J., Cao, C.-Y.,
872 2013. Ca. 1.5Ga mafic magmatism in South China during the break-up of the
873 supercontinent Nuna/Columbia: The Zhuqing Fe-Ti-V oxide ore-bearing mafic
874 intrusions in western Yangtze Block. Lithos, 168-169, 85-98.
875 Fezaa, N., Liégeois, J.P., Abdallah, N., Bruguier, O., Laouar, R., Ouabadi, A., 2013. Origine
876 du groupe métasédimentaire de Djanet (Hoggar oriental, Algérie). Géochronologie et
877 géochimie. Bulletin du Service Géologique National, 24, 3-26.
878 Fezaa, N, Liégeois, J.-P., Abdallah, N., Cherfouh, E.H., De Waele, B., Bruguier, O. Ouabadi,
879 A. 2010. The Djanet terrane (Eastern Hoggar, Algeria), the Pan-African metacratonic
880 boundary of the Murzuq craton: field, detrital and magmatic U-Pb zircon and Sr-Nd
881 isotopes evidences. Precambrian Research 180, 299–327
882 Fisher, R.A., 1953. Dispersion on a sphere. Proceedings of the Royal Society, London *A* 217,
883 295-305.
884 Foulger G., Hamilton W.R., 2014. Earth science: Plume hypothesis challenged. Nature 505,
885 618.
886 Freulon J.M., 1964. Etudes géologiques des séries primaires du Sahara Central (Tassili n'Ajjer
887 et Fezzan). Publication du Centre de Recherches sur les Zones Arides, CNRS Paris,
888 Géologie, 3.
889 Fröhlich, S., Petitpierre, L., Redfern, J., Grech, P., Bodin, S., Lang, S., 2010.
890 Sedimentological and sequence stratigraphic analysis of Carboniferous deposits in
891 western Libya: Recording the sedimentary response of the northern Gondwana margin
892 to climate and sea-level changes. Journal of African Earth Sciences 57, 279–296.
893 Galeazzi, S., Point, O., Haddadi, N., Mather, J., Druesne D., 2010. Regional geology and
894 petroleum systems of the Illizi–Berkine area of the Algerian Saharan Platform: An
895 overview. Marine and Petroleum Geology 27,143–178.
896 Geological Map of Libya, 1985, SW sheet. Compiled by industrial Research Centre,
897 Geological Research and Min. Department, Tripoli, Libya.
898 Ghienne, J.F., Moreau, J., Degermann, L., Rubino, J.L., 2013. Lower Palaeozoic
899 unconformities in an intracratonic platform setting: glacial erosion versus tectonics in
900 the eastern Murzuq Basin (southern Libya). International Journal of Earth Sciences,
901 102, 455-482.
902 Guiraud, R, Bosworth, W., Thierry, J. Delplanque, J.A., 2005. Phanerozoic geological
903 evolution of Northern and Central Africa: An overview. Journal of African Earth
904 Sciences 43 (2005) 83–143
905 Haddoum, H., Guiraud, R., Moussine-Pouchkine, A. 2001. Hercynian compressional
906 deformations of the Ahnet-Mouydir Basin, Algerian Saharan Platform: far-field stress
907 effects of the Late Palaeozoic orogeny. Terra Nova 13, 220–226.
908 Hargraves, R.B., Dawson, E.M. and Houten, F.B., 1987. Palaeomagnetism and age of mid-
909 Palaeozoic ring complexes in Niger, West Africa, and tectonic implications.
910 Geophysical Journal of the Royal Astronomical Society 90, 705-729.
911 doi: 10.1111/j.1365-246X.1987.tb00750.x
912 Heine, C., Müller, R.D., Steinberger, B., Torsvik, T.H., 2008. Subsidence in intracontinental
913 basins due to dynamic topography. Physics of the Earth and Planetary Interiors 171,
914 252–264.
915 Henry, B., Merabet, N., Derder, M.E.M. and Bayou, B. 2004. Chemical remagnetizations in
916 the Illizi basin (Saharan craton, Algeria). Geophysical Journal International, 156: 200-
917 212.

Henry, B., Liégeois J.P., Nouar, O., Derder, MEM, Bayou, B., Bruguier, O., Ouabadi, A., Belhai, D., Amenna, M., Hemmi, A., Ayache, M., 2009. Repeated granitoid intrusions during the Neoproterozoic along the western boundary of the Saharan metacraton, Eastern Hoggar, Tuareg shield, Algeria: An AMS and U–Pb zircon age study. Tectonophysics, 474, 417-434.

Henry, B., Derder, M.E.M., Amenna, M., Maouche, S. Bayou, B., Ouabadi, A., Bouabdallah, H., Ayache, M., Beddiaf, M., Bestandji, R., 2014. Paleomagnetic dating of continental geological formations: Strong diachronism evidenced in the Saharan platform and geodynamical implications. Journal of African Earth Sciences, 99, 353-362. doi: 10.1016/j.jafrearsci.2014.02.010.

Henry, B., Derder, M.E.M., Amenna, M., Maouche, S., Bayou, B., 2015. More accurate selection of the paleomagnetic poles for APWPs building: a step towards better geodynamical reconstructions - case study of the Western Gondwana. Geophysical Journal International, submitted.

Kirschvink, J.L., 1980. The least-squares line and plane and the analysis of palaeomagnetic data. Geophysical Journal of the Royal astronomical Society, 62, 699-718.

Khudoley, A.K., Prokopiev, A.V., Chamberlain, K. R., Ernst, R.E., Jowitt, S. M., e, Malyshev, S.V.,Zaitsev, A.I., Kropachev, A.P., Koroleva, O.V., 2013. Early Paleozoic mafic magmatic events on the eastern margin of the Siberian Craton. Lithos 174, 44–56.

LeBas, M.J., LeMaitre, R.W., Streckeisen, A., Zanettin, B., 1986. A chemical classification of volcanic rocks based on the total alkali–silica diagram. Journal of Petrology, 27, 745–750.

Le Caignec. J., Harel, M., Didier, J., Illy, P., 1957. Reports of the BRMA (Bureau de Recherches Minières de l'Algérie)for Djanet area, Mission Illy (Hoggar 1956-1957), Feuilles au 1/200 000 : Fort Charlet et Tin Alkoum.

Legrand, P., 2000. Une région de référence pour la limite Ordovicien–Silurien : l'Oued In Djerane, Sahara algérien. Comptes Rendus de l'Académie des Sciences - Series IIA - Earth and Planetary Science, 330 :61-66

Léger, J.M., 1985. Géologie et évolution magmatique du complexe plutonique d'Iskou (Aïr, Niger). Journal of African Earth Sciences, 3, 89-96

Lelubre M., Freulon, J.M., Lefranc, P., 1962. Carte géologique du Nord-Ouest de l'Afrique, feuille Sahara central, 1/2,000,000ème. CNRS, France.

Le Maitre, R.W., Streckeisen, A., Zanettin, B., Le Bas, M.J., Bonin, B., Bateman, P., Bellieni, G., Dudek, A., Efremova, S., Keller, J., Lameyre, J., Sabine, P.A., Schmid, R., Sorensen, H., Woolley, A.R., 2002. Igneous Rocks: A Classification and Glossary of Terms: Recommendations of the International Union of Geological Sciences. Subcommission on the Systematics of Igneous Rocks. Cambridge University Press, 236 pp.

Linnemann, U., Ouzegane, K., Drareni, A., Hofmann, M., Becker, S., Gärtner, A., Sagawe, A., 2011. Sands of West Gondwana: An archive of secular magmatism and plate interactions. A case study from the Cambro-Ordovician section of the Tassili Ouan Ahaggar (Algerian Sahara) using U–Pb–LA-ICP-MS detrital zircon ages. Lithos, 123, 188–203.

Liégeois, J.P., Latouche, L., Boughrara, M., Navez, J., Guiraud, M., 2003. The LATEA metacraton (Central Hoggar, Tuareg shield, Algeria): behaviour of an old passive margin during the Pan-African orogeny. Journal of African Earth Sciences 37, 161–190.

Liégeois, J.P., Benhallou, A., Azzouni-Sekkal, A., Yahiaoui, R., Bonin, B., 2005. The Hoggar swell and volcanism: reactivation of the Precambrian Tuareg shield during Alpine

convergence and West African Cenozoic volcanism. In: Foulger, G.R., Natland, J.H., Presnall, D.C., Anderson, D.L. (Eds.), Plates, Plumes and Paradigms: Geological Society of America Special Paper, 388. 379–400.

Liégeois, J. P., Abdelsalam, M. G., Ennih, N., Ouabadi, A. 2013. Metacraton: Nature, genesis and behaviour. Gondwana Research 23, 220–237

Lustrino, M., Cucciniello, C., Melluso, L., Tassinari, C.C.G., De Gennaro, R., Serracino, M., 2012. Petrogenesis of Cenozoic volcanic rocks in the NWsector of the Gharyan volcanic field, Libya. Lithos 155, 218–235.

MacDonald, G.A. and Katsura, T., 1964. Chemical compositions of Hawaiian lavas. Journal of Petrology, 5, 82-133

Marzoli, A., Renne, P.R., Piccirillo, E.M., Ernesto, M., Bellieni, G., DeMin, A., 1999. Extensive 200-million-year-old continental flood basalts of the Central Atlantic Magmatic Province. Science 284, 616–618.

Massa, D., Coquel, R., Doubinger, R., 1988. New Palynological Data on the Visean/Moscovian Carboniferous Interval in the Ghadames Basin (Libya). Comparison with Saharan Basins. Assesment of the Gondwanian and Euramerican Influences. Oil & Gas Science Technology, Revue de l'Institut Français du Pétrole, 43, 3-16.

Michard, A., Hoepffner, C., Soulaimani, A., Baidder, L., 2008. The Variscan Belt. In: A. Michard et al., Continental Evolution: The Geology of Morocco. Lecture Notes in Earth Sciences, 116, 65-131.

Moreau, C., Demaiffe, D., Bellion, Y. and Boullier, A.M., 1994. A tectonic model for the location of Paleozoic ring-complexes in Aïr (Niger, West Africa). Tectonophysics, 234, 129-146.

Moreau, J., Ghienne, J.F., Hurst, A., 2012. Kilometre-scale sand injectites in the intracratonic Murzuq Basin (south-west Libya): an igneous trigger? Sedimentology, 59: 1321-1344.

Morton, A.C, Meinhold, G., Richard, J.P., Phillips, J., Strogen, D., Abutarruma, Y., Elgadry, M., Thusu, B., A.G., 2011. A heavy mineral study of sandstones from the eastern Murzuq Basin, Libya: Constraints on provenance and stratigraphic correlation. Journal of African Earth Sciences 61, 308–330.

Nelson, S.A. and Carmichael, I.S.E., 1984. Pleistocene to recent alkalic volcanism in the region of Sanganguey volcano, Nayarit, Mexico. Contributions to Mineralogy and Petrology, 85, 321 - 335.

Nouar, O., Henry, B., Liégeois, J.P., Derder, M.E.M., Bayou, B., Bruguier, O., Ouabadi, A., Amenna, M., Hemmi, A., Ayache, M., 2011. Eburnean and Pan-African granitoids and the Raghane mega-shear zone evolution: Image analysis, U-Pb zircon age and AMS study in the Arokam Ténéré (Tuareg shield, Algeria), Journal of African Earth Sciences, 60, 133-152.

Pearce, J., 1982. Role of the sub-continental lithosphere in magma genesis at active continental margins. In: Hawkesworth, C.J. and Norry, M.J. (eds) Continental basalts and mantle xenoliths. Shiva Geology Series, Nantwich, 230-249.

Radivojević, M., Toljić, M., Turki, S.M., Bojić, Z., Šarić, K., Cvetković, V., 2015. Neogene to Quaternary basalts of the Jabal Eghei (Nuqay) area (south Libya): Two distinct volcanic events or continuous volcanism with gradual shift in magma composition? Journal of Volcanology and Geothermal Research 293, 57–74

Rapalini, A.E., Vilas, J.F., 1991. Preliminary paleomagnetic data from the Sierra Grande Formation: tectonic consequences of the first mid-Paleozoic paleopoles from Patagonia. Journal of South American Earth Sciences, 4: 25-41

Reimold, W.E., Koeberl, C., 2014. Impact structures in Africa: A review. Journal of African Earth Sciences, 93, 57-175.

1018 Ritzmann, O., Faleide, J.I., 2009. The crust and mantle lithosphere in the Barents Sea/Kara
1019 Sea region. Tectonophysics 470, 89–104.
1020 Rogers N.W., James D., Kelley S.P., de Mulder M., 1998. The generation of potassic lavas
1021 from the eastern Virunga Province, Rwanda. Journal of Petrology, 39: 1223–1247.
1022 Schmidt, P.W., Embleton, B.J.J., Palmer, H.C., 1987. Pre- and post-folding magnetizations
1023 from the early Devonian Snowy River Volcanics and Buchan Caves Limestone,
1024 Victoria. Geophysical Journal International, 91: 155-170.
1025 Schulmann, K., Martinez Catalan, J. R., Lardeaux, J. M., Janousek, V., Oggiano, G.,, 2014.
1026 The Variscan Orogeny: Extent, Timescale and the Formation of the European Crust.
1027 Geological Society, London, Special Publications, 405, 1–6.
1028 Smith, B., Derder, M.E.M., Henry, B., Bayou, B., Yelles, A.K., Djellit, H., Amenna, M.,
1029 Garces, M., Beamud, E., Callot, J.P., Eschard, R., Chambers, A., Aifa, T., Ait Ouali,
1030 R., Gandriche, H., 2006. Relative importance of the Hercynian and post-Jurassic
1031 tectonic phases in the Saharan platform: A palaeomagnetic study of Jurassic sills in the
1032 Reggane Basin (Algeria). Geophysical Journal International, 167, 380-396.
1033 Stampfli, G.M., Borel, G.D., 2002. A plate tectonic model for the Paleozoic and Mesozoic
1034 constrained by dynamic plate boundaries and restored synthetic oceanic isochrons.
1035 Earth and Planetary Science Letters 196, 17-33.
1036 Steiger, R.H., Jäger, E., 1977. Subcommission on geochronology: convention on the use of
1037 decay constants in geo- and cosmo-chronology. Earth and Planetary Science Letters
1038 36, 359-362.
1039 Sun, S.S., 1980. Lead isotopic study of young volcanic rocks from mid-ocean ridges, ocean
1040 islands and islands arcs. Philosophical Transactions Royal Society London A297,
1041 409–445
1042 Sun, S.S., McDonough, W.F., 1989. Chemical and isotopic systematics of oceanic basalts:
1043 implications for mantle compositon and processes. In: Saunders, A.D., Norry, M.J.
1044 (Eds.), Magmatism in Ocean Basins, Geological Society of London Special
1045 Publication 42, pp. 313-345.
1046 Taylor, S.R., Mc Lennan, S.M., 1985. The continental Crust: Its Composition and Evolution.
1047 Blakwell, Oxford, 312 pp.
1048 Torsvik, T.H., van der Voo, R., Preeden, U., Mac Niocaill, C., Steinberger, B., Doubrovine,
1049 P.V., van Hinsbergen, D.J.J., Domeier, M., Gaina, C., Tohver, E., Meert, J.G.,
1050 McCausland, P.J.A., Cocks, L.R. M., 2012. Phanerozoic polar wander,
1051 paleogeography and dynamics. Earth-Science Reviews 114, 325-368,
1052 doi:10.1016/j.earscirev.2012.06.007
1053 Wanless, V.D., Garcia, M.O., Rhodes, J.M., Weis, D., Norman, M.D., 2006. Shield-stage
1054 alkalic volcanism on Mauna Loa Volcano, Hawaii. Journal of Volcanology and
1055 Geothermal Research, 151, 141–155.
1056 Watson, E.B., Harrison, T.M., 1983. Zircon saturation revisited: temperature and composition
1057 effects in a variety of crustal magma types. Earth and Planetary Science Letters 64,
1058 295–304.
1059 Wiedenbeck, M., Alle, P., Corfu, F., Griffin, W.L., Meier, M., Oberli, F., von Quadt, A.,
1060 Roddick, J.C., Spiegel, W., 1995. Three natural zircon standards for U-Th-Pb, Lu-Hf,
1061 trace element and REE analyses. Geostandards Newsletter 19, 1-23.
1062 Wilson, R.L., Everitt, C.W.F., 1963. Thermal demagnetization of some Carboniferous lavas
1063 for paleomagnetic purposes. Geophysical Journal of the Royal Astronomical Society
1064 8, 149–164.
1065 Winchester, J.A., Floyd, P.A., 1977. Geochemical discrimination of different magma series
1066 and their differentiation products using immobile elements. Chemical Geology, 20,
1067 325–343.

1068 Yahiaoui R., Dautria J.-M., Allard O., Bosch D., Azzouni-Sekkal A., Bodinier J.-L., 2014. A
1069 volcanic district between the Hoggar uplift and the Tenere Rifts: Volcanology,
1070 geochemistry and age of the In-Ezzane lavas (Algerian Sahara). Journal of African
1071 Earth Sciences, 92, 14-20.
1072 Zhang, J., Huang, Z., Luo, T., Qian, Z., Zhang, Y., 2013. Origin of early Triassic rift related
1073 alkaline basalts from Southwest China: age, isotope, and trace-element constraints,
1074 International Geology Review, 55, 1162-1178.
1075 Zijderveld, J.D.A., 1967. AC demagnetisation of rocks: analysis of results. In: Collinson,
1076 D.W., Creer, K.M., Runcorn, S.K. (Eds.), Method in paleomagnetism. Elsevier.
1077 Amsterdam, 254-286.
1078

1079 **Figure caption**

1080 Figure 1: Geological map of the southwestern Murzuq basin margin: A) Location in the North
1081 African context based on Lelubre et al., 1962; Liégeois et al., 2003, 2005; Fezaa et al.,
1082 2010. White rectangles indicate the circular structures discussed in the text: Mt T.=
1083 Mount Telout; I.E.= In-Ezzane; El Meh.= El Meherschema. B) Geological map of the
1084 studied area (modified after Le Caignec et al, 1957, Fezaa et al., 2010 and Geological
1085 Map of Libya, 1985, SW sheet).

1086 Figure 2: Detailed map of the Arrikine sill, from image analysis through Landsat 8 satellite
1087 images and from field observations and measurements: a) Names on the map concern
1088 geographical location of the two main “oueds” in this area. A color composite
1089 analysis, using TM6, TM3 and TM1 bands with contrast enhancement, highlights a
1090 NW-SE dark band corresponding to magmatism observed and sampled on the field.
1091 Contrasting spectral responses allow differentiating the Silurian clays in purple and the
1092 Devonian sandstones in brown. b) Names on the map concern geological formations.
1093 The relative homogeneity of responses within these different areas, leads us to try to
1094 specify the extension and edges of the sill. Four classes have been defined (green
1095 clays, marls and limestones; red dark rocks; brown sandstones; white alluvial
1096 material). The result is a classified image by maximum likelihood method. The
1097 Cambro-Ordovician levels are not differentiated by this classification and the
1098 magmatism in red is well underlined with its NW-SE orientation. However, the
1099 northern part of the red area shows a surprising lateral eastward extension.
1100 Comparison with the figure 2a rather suggests drainage of dark material by the Oued
1101 Arrikine. The paleomagnetic sampling sites are indicated with numbers by yellow
1102 squares (gabbro) and black dots (sedimentary formations). Cambro-Ordovician (ks),
1103 Silurian (s) with its two formations (Oued In Djerane and Acacus) and Devonian (d).
1104 Yellow circles correspond to injectites.

Figure 3: U-Pb concordia diagram.

Figure 4: Thermal demagnetization curves for representative samples of the dark facies.

Figure 5: Typical thermomagnetic curves (normalized low field susceptibility K/K_o as a function of the temperature T - in °C) for representative samples of the gray (IZ716) and dark (IZ696) facies of the gabbro.

Figure 6: a, b): Hysteresis loops (a: sample IZ725 and b: sample IZ678, both for dark facies); Hcr is the remanent coercive force, Field H in Tesla. c) Day plot (Day et al. 1977) of the hysteresis ratios; PSD (pseudo-single domain) and MD (multidomain) areas for magnetite.

Figure 7: Orthogonal vector plots (filled circles: horizontal plane, crosses: vertical plane), in stratigraphic coordinates for AF (a, c and e), thermal (b, d, f) and mixed (g) treatments for samples IZ659A (a), IZ664A (b), IZ709A (c), IZ739A (d), IZ711A and B (e, f) and IZ660A (g).

Figure 8: Equal-area plot after dip correction (a) of ChRMs C and (b) of the mean-site paleomagnetic directions with associated 95% confidence zone (open circles: negative inclinations).

Figure 9: In North-West Africa coordinates, comparison of the Arrikine pole with Lower Devonian poles (see text), with the 560-210 Ma Gondwana APWP (in red 560-250 Ma - Amenna et al., 2014, Henry 2015 – in orange 240-210 Ma - Domeier et al., 2012), the Africa APWP (in green 200-0 Ma - Besse and Courtillot, 2002) and in blue the 430-380 Ma Gondwana APWP of Torsvick et al. (2012). Paleomagnetic poles with associated confidence zone of Mt. Leyshon Devonian dykes (Mt. LDD) in Australia (Clarck, 1996), Snowy River Volcanics (SRV) in Australia (Schmidt et al., 1987), Herrada Member, Sierra Grande (HM) in Argentina (Rapalini and Vilas, 1991), Aïr intrusives (Aïr) in Niger (Hargraves et al., 1987), Tin Serririne (TS – Derder et al., 2006) and Arrikine (ARK) in Algeria (this study). Confidence zones are also presented for the 250 or 500 Ma poles of the APWPs.

Figure 10: Arrikine sill representative sample AF-ALG/Dj-Site58 compared with rocks having also a high-Ti basaltic composition (Aïr, Niger (Abontorok ring-complex): Brown et al., 1989; Siberia: Khudoley et al., 2013, Virunga: Rogers et al., 1998, Hawaii: Wanless et al., 2006, Yangtse: Fan et al., 2013, SW China: Zhang et al., 2013). (A) REE normalized to chondrites (Taylor and McLennan, 1985), (B) Dj 58 spectrum for incompatible elements normalized to MORB (Sun, 1980 and Pearce,

1982) compared with high-Ti basaltic composition of rocks of Siberia, Virunga, Hawaii, Yangtse and SW China (see references above)

Figure 11: Arrikine gabbro AF-ALG/Dj-Site58 spectrum for incompatible elements normalized to the Primitive Mantle (Sun and McDonough, 1989) compared with Siberian high-Ti basalts (Suordakh event, Eastern margin of the Siberian craton; Khudoley et al., 2013).

Table 1: Microprobe analysis

Table 2: K-Ar dating of the Arrikine sill.

Table 3: U-Th-Pb laser ablation ICP-MS analyses for zircons extracted from the Arrikine gabbro.

Table 4: Mean direction: Site, number of ChRM N, Declination D and Inclination I before and after dip correction, Fisher (1953) parameters k and $\alpha_{95,}$ and VGP or paleomagnetic pole: Lat. (°S), Long (°E), with for the latter corresponding Fisher parameters K and A_{95}.

Table 5: Major and trace elements for the Arrikine sill measured on a Horiba-Jobin-Yvon Ultima 2 ICP-AES at the IUEM, Pôle de Spectrométrie Océan, Brest, France, by Céline Liorzou. CIPW norm and other parameters have been calculated using Norm4 Excel spreadsheet from Kurt Hollocher: (http://minerva.union.edu/hollochk/c_petrology/norms.htm).

Mineral		SiO_2	TiO_2	Al_2O_3	FeO	MnO	MgO	CaO	Na_2O	K_2O	P_2O_5	Cr_2O_3	NiO	BaO	Total
	Magmatic minerals														
Plagioclase	58 A-8	54.43	0.150	28.51	0.316	0.000	0.056	11.33	4.933	0.328	0.060	0.000	0.000	0.081	100.19
Pyroxène	58 B-2	50.76	1.027	1.252	12.818	0.246	11.16	21.99	0.506	0.014	0.000	0.002	0.000	0.025	99.81
Biotite	58 B-1	34.86	6.895	12.86	24.52	0.162	7.943	0.000	0.441	9.051	0.011	0.000	0.000	0.000	96.74
Biotite	58 A-5	34.99	7.247	13.53	21.42	0.087	9.491	0.040	0.688	9.068	0.000	0.000	0.000	0.000	96.57
Apatite	58 A-4	0.473	0.000	0.068	0.496	0.048	0.112	54.80	0.003	0.000	42.49	0.000	0.000	0.043	98.53
Opaque	58 A-6	0.005	52.51	0.069	45.22	0.684	1.636	0.051	0.000	0.000	0.000	0.000	0.002	0.000	100.17
Opaque	58 A-7	0.070	26.62	1.269	67.61	1.398	0.014	0.049	0.008	0.006	0.010	0.000	0.001	0.000	97.06
	Aplitic secondary minerals														
Hyper-K spot	58 B-1	64.33	0.000	18.42	0.039	0.003	0.051	0.097	0.837	15.57	0.005	0.000	0.008	0.260	99.61
Hyper -K-Ba spot	58 B-1	61.97	0.073	20.09	0.201	0.000	0.003	0.832	2.837	9.821	0.000	0.000	0.000	3.481	99.30
High-K spot	58 B-1	65.10	0.125	21.12	0.172	0.015	0.003	2.206	8.490	2.801	0.000	0.000	0.000	0.098	100.13
	Altered Fe-Mg minerals														
Altered spot	58 A-1	37.97	0.146	2.455	23.85	0.195	6.631	10.80	0.139	0.206	3.912	0.000	0.000	0.000	86.30
Altered spot (brown)	58 A-2	31.03	0.025	12.26	29.37	0.179	14.40	0.340	0.029	0.029	0.000	0.000	0.013	0.000	87.67
Altered spot (green)	58 A-3	31.86	0.057	11.26	30.80	0.129	13.52	0.447	0.105	0.045	0.000	0.000	0.000	0.034	88.25

Sample code	Lab. anal. ref.	Age (Ma)	±	error at ± 1 σ	K_2O wt. %	$^{40}Ar_R$ ($10^{-5}cm^3 g^{-1}$)	$^{40}Ar_R$ (%)	Fused weight (g)	$^{36}Ar_{exp}$ ($10^{-10}cm^3$)
AF-ALG/Dj-Ste58	B 7398-1	327.2	±	7.6	1.40	1.619	85.3	0.4042	38.2
	B 7399-2	314.2	±	7.3		1.549	86.8	0.3008	23.4
	B 7437-8	333.5	±	7.7		1.654	86.7	0.0580	5.00
	B 7459-11	327.9	±	7.6		1.623	83.4	0.0729	7.96
	Mean age	**325.6**	**±**	**7.7**					

Sample	Pb* (ppm)	Th (ppm)	U (ppm)	Th/U	$^{208}Pb/^{206}Pb$	$^{207}Pb/^{206}Pb$	± (1σ)	$^{207}Pb/^{235}U$	± (1σ)	$^{206}Pb/^{238}U$	± (1σ)	Rho	Apparent age (Ma)				Conc (%)
													$^{206}Pb/^{238}U$	± (1σ)	$^{207}Pb/^{206}Pb$	± (1σ)	
Arrikine gabbro																	
#1-1	87	82	142	0.58	0.16	0.18473	0.00207	13.247	0.112	0.5197	0.0041	0.94	2698	18	2696	18	100.1
#2-1	44	17	421	0.04	0.02	0.06024	0.00094	0.856	0.011	0.1030	0.0009	0.64	632	5	612	34	103.2
#2-2	25	7	247	0.03	0.02	0.12609	0.00177	6.777	0.078	0.3895	0.0037	0.82	2121	17	2044	25	103.7
#3-1	219	112	523	0.21	0.07	0.18420	0.00221	13.218	0.124	0.5201	0.0045	0.92	2700	19	2691	20	100.3
#4-1	134	151	213	0.71	0.19	0.12365	0.00147	6.635	0.061	0.3889	0.0032	0.88	2118	15	2010	21	105.4
#5-1	664	113	1037	0.11	0.02	0.18601	0.00217	13.412	0.121	0.5227	0.0044	0.93	2711	19	2707	19	100.1
#6-1	96	118	155	0.77	0.22	0.12506	0.00137	6.572	0.054	0.3809	0.0029	0.93	2081	13	2030	19	102.5
#7-1	308	84	804	0.10	0.04	0.06124	0.00189	1.066	0.030	0.1262	0.0017	0.46	766	10	648	65	118.3
#8-1	8	19	62	0.31	0.10	0.12485	0.00138	6.397	0.053	0.3715	0.0028	0.92	2036	13	2027	20	100.5
#9-1	12	56	103	0.55	0.16	0.06410	0.00108	0.946	0.014	0.1070	0.0010	0.63	656	6	745	35	88.0
#10-1	16	102	130	0.78	0.25	0.06221	0.00149	0.945	0.021	0.1102	0.0012	0.50	674	7	681	50	98.9
#11-1	10	38	91	0.41	0.14	0.06207	0.00129	0.955	0.018	0.1116	0.0011	0.54	682	6	676	44	100.9
#12-1	22	143	177	0.81	0.25	0.12459	0.00135	6.088	0.049	0.3543	0.0027	0.94	1955	13	2023	19	96.7
#13-1	648	127	1628	0.08	0.02	0.06548	0.00159	1.004	0.022	0.1112	0.0012	0.50	680	7	790	50	86.1
#13-2	338	72	1007	0.07	0.02	0.06236	0.00116	0.970	0.016	0.1129	0.0011	0.57	690	6	686	39	100.5
#14-1	7	47	68	0.69	0.21	0.05945	0.00195	0.796	0.024	0.0972	0.0012	0.42	598	7	584	70	102.4
#15-1	106	58	327	0.18	0.06	0.13819	0.00152	6.015	0.049	0.3158	0.0024	0.93	1769	12	2205	19	80.2
#16-1	466	204	1162	0.18	0.05	0.12585	0.00135	6.459	0.051	0.3724	0.0028	0.94	2041	13	2041	19	100.0
#17-1	567	210	1533	0.14	0.05	0.12481	0.00132	6.358	0.049	0.3696	0.0027	0.95	2027	13	2026	19	100.1

Table 3: U-Th-Pb laser ablation ICP-MS analyses for zircons extracted from the Arrikine gabbro

		Before and after dip correction						***PGVs*** and **Paleomagnetic pole**			
Site	N	D(°)	I(°)	D(°)	I(°)	k	α_{95}(°)	Lat(°S)	Long(°E)	K	A_{95}(°)
50	6	357.4	-24.7	354.6	-25.2	40	10.8	***52.4***	***19.1***		
51	3	342.6	-47.4	336.3	-46.3	416	6.1	***33.5***	***35.8***		
52	6	10.7	-45.7	4.6	-47.4	27	13.1	***37.3***	***5.4***		
53	9	357.8	-37.1	353.2	-37.5	109	4.9	***44.5***	***19.4***		
54	9	349.8	-36.2	345.4	-35.8	118	4.8	***43.9***	***29.7***		
55	2	-	-	-	-	-	-	**-**	**-**		
56	1	-	-	-	-	-	-	**-**	**-**		
57	10	355.8	-36.1	352.9	-36.5	66	6.0	***45.2***	***20.0***		
58	6	347.9	-35.2	343.7	-34.7	72	7.9	***44.1***	***32.2***		
59	7	2.7	-45.5	356.6	-46.4	44	9.2	***38.2***	***14.3***		
60	12	353.7	-36.0	349.3	-36.0	115	4.1	***44.8***	***24.7***		
61	13	351.1	-41.6	345.8	-41.3	21	9.4	***40.3***	***27.6***		

Mean (specimens)	84	355.4	-38.4	350.7	-38.6	38	2.5				
Mean (Sites)	10	355.5	-38.8	350.6	-38.9	86	5.2	**42.8**	**22.9**	**88**	**4.7**

Sample AF-ALG / Dj 58

Oxide	a %	b %
SiO_2	43.80	45.99
TiO_2	4.77	5.01
Al_2O_3	13.97	14.66
Fe_2O_3	15.94	16.73
MnO	0.19	0.20
MgO	3.90	4.10
CaO	6.28	6.60
Na_2O	4.12	4.32
K_2O	1.40	1.47
P_2O_5	0.87	0.91
LOI	1.84	1.84
Total	97.11	97.11

a Analysis
b Analysis recalculated to 100% on an anhydrous basis

Element	ppm
Rb	27.2
Sr	442
Ba	1247
Sc	19.3
V	171
Cr	3
Co	46
Ni	39
Y	38.6
Zr	320
Nb	32.7
La	37.7
Ce	84.0
Nd	48.9
Sm	9.9
Eu	3.3
Gd	9.6
Dy	7.7
Er	3.8
Yb	3.3
Th	2.3

Normative minerals	Vol %
Plagioclase	60.47
Orthoclase	11.05
Diopside	8.16
Hypersthene	1.13
Olivine	5.64
Ilmenite	6.13
Magnetite	5.36
Apatite	2.02
Zircon	0.04
Plagioclase An content	29.15
Differentiation Index	62.31
Calculated density, g/cc	3.03
Calculated liquid density, g/cc	2.70
Calculated viscosity, dry, Pas	0.17
Calculated viscosity, wet, Pas	0.16
Estimated liquidus temp,, °C	1280
Estimated H2O content, wt, %	0.20

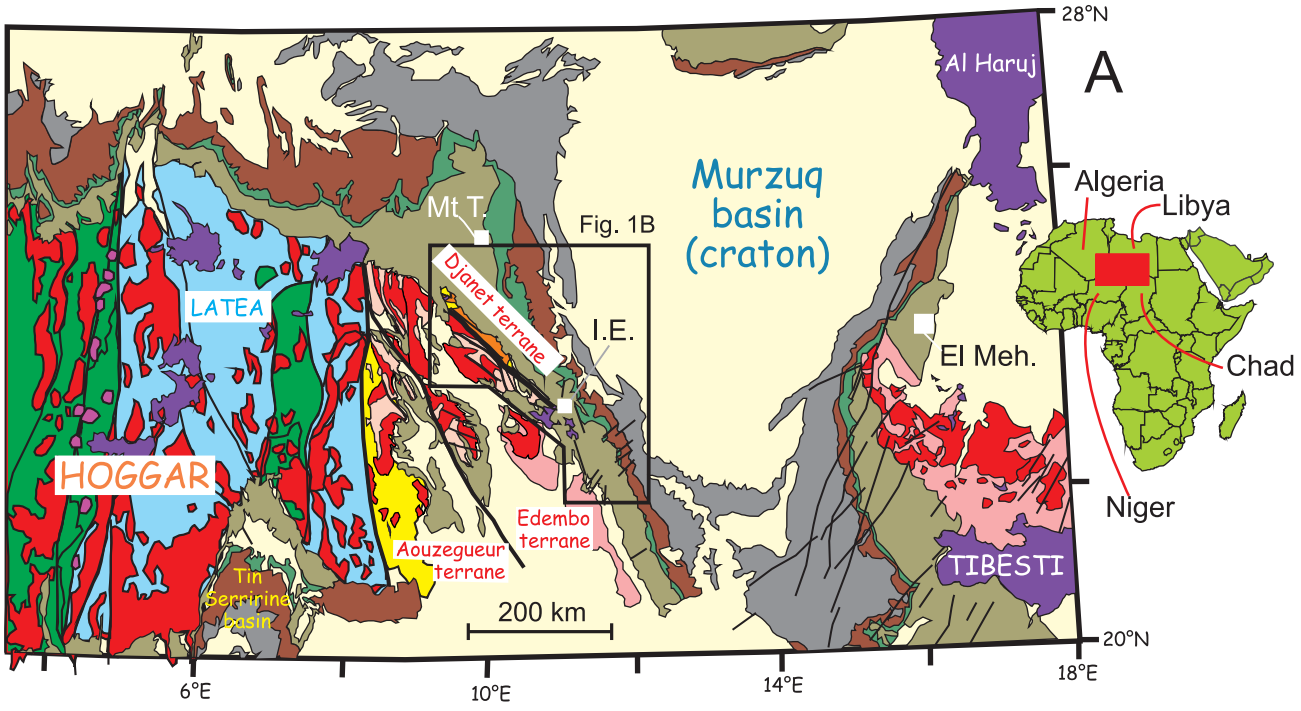
A
Al Haruj
Murzuq basin (craton)
Mt T.
Fig. 1B
Djanet terrane
I.E.
LATEA
HOGGAR
Edembo terrane
Aouzegueur terrane
Tin Serrinine basin
TIBESTI
El Meh.
Algeria
Libya
Chad
Niger
200 km
28°N
20°N
6°E
10°E
14°E
18°E

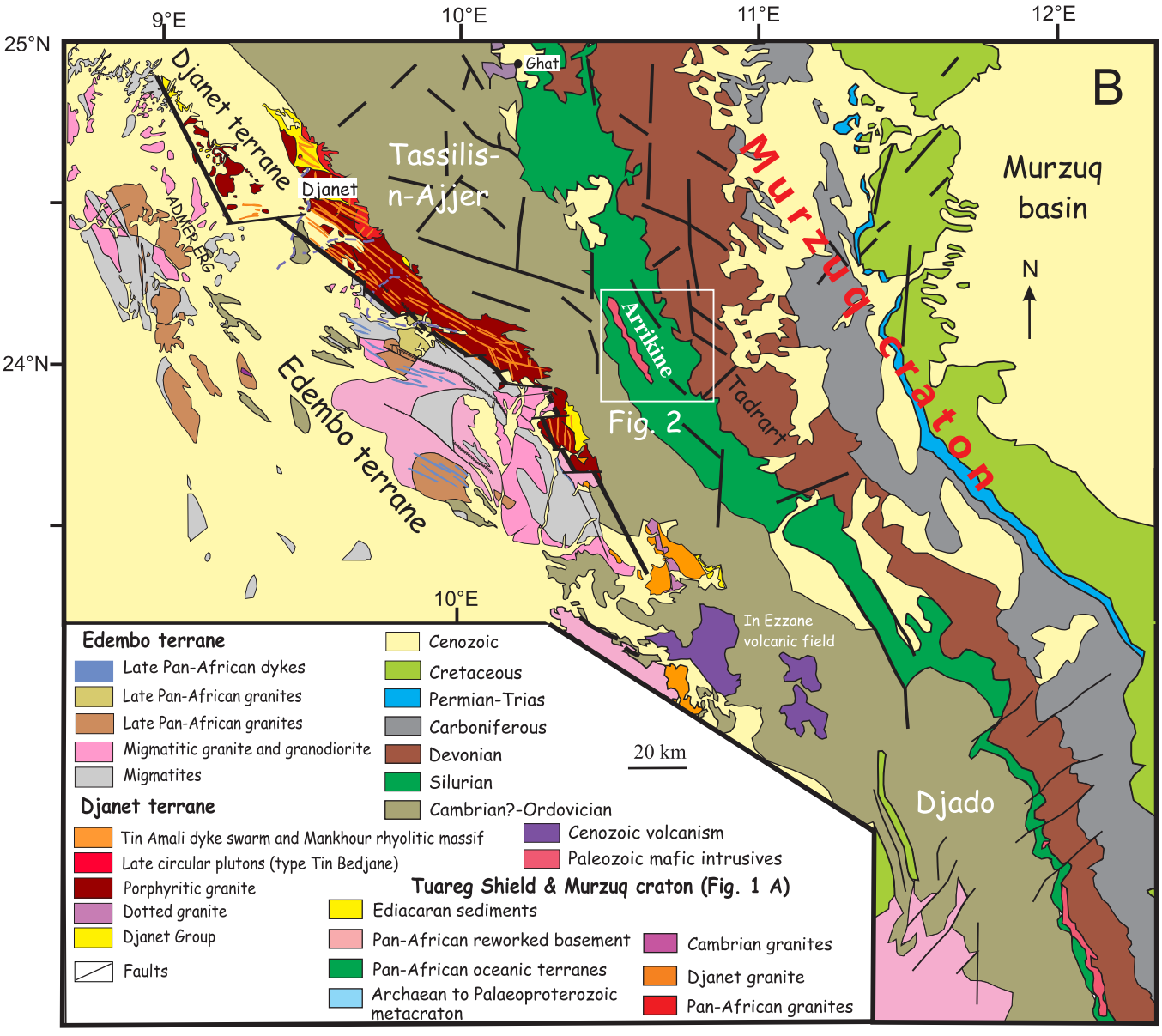
B
9°E
10°E
11°E
12°E
25°N
24°N
Djanet terrane
Djanet
ADMER ERG
Ghat
Tassilis-n-Ajjer
Murzuq basin
Murzuq craton
N
Arrikine
Fig. 2
Tadrart
Edembo terrane
In Ezzane volcanic field
Djado
20 km
Edembo terrane
Late Pan-African dykes
Late Pan-African granites
Late Pan-African granites
Migmatitic granite and granodiorite
Migmatites
Djanet terrane
Tin Amali dyke swarm and Mankhour rhyolitic massif
Late circular plutons (type Tin Bedjane)
Porphyritic granite
Dotted granite
Djanet Group
Faults
Cenozoic
Cretaceous
Permian-Trias
Carboniferous
Devonian
Silurian
Cambrian?-Ordovician
Cenozoic volcanism
Paleozoic mafic intrusives
Tuareg Shield & Murzuq craton (Fig. 1 A)
Ediacaran sediments
Pan-African reworked basement
Pan-African oceanic terranes
Archaean to Palaeoproterozoic metacraton
Cambrian granites
Djanet granite
Pan-African granites

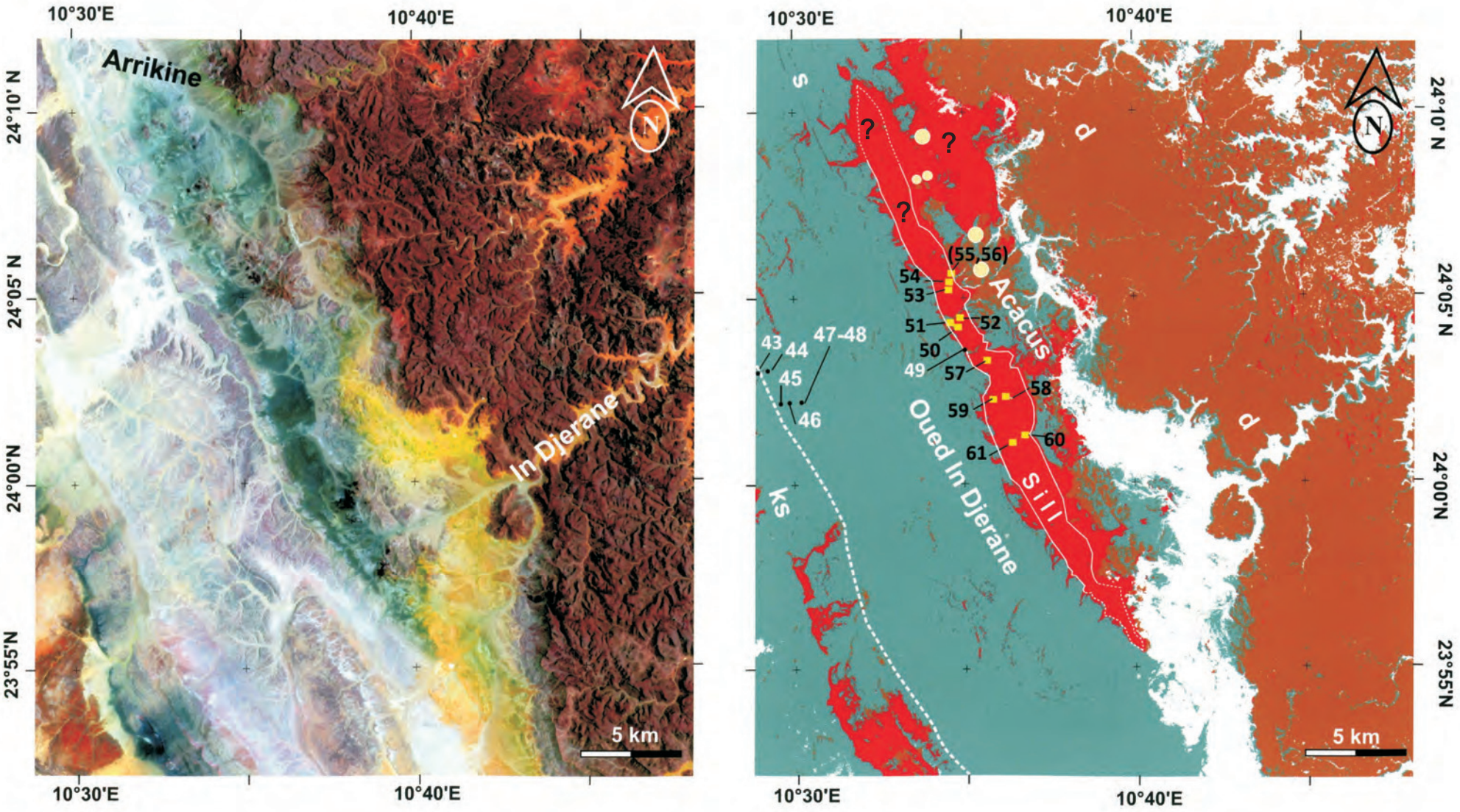
10°30'E
10°40'E
24°10' N
24°05' N
24°00'N
23°55'N
Arrikine
In Djerane
N
5 km
s
d
ks
?
(55,56)
54
53
52
51
50
49
57
58
59
60
61
47-48
43
44
45
46
Acacus
Oued In Djerane
Sill

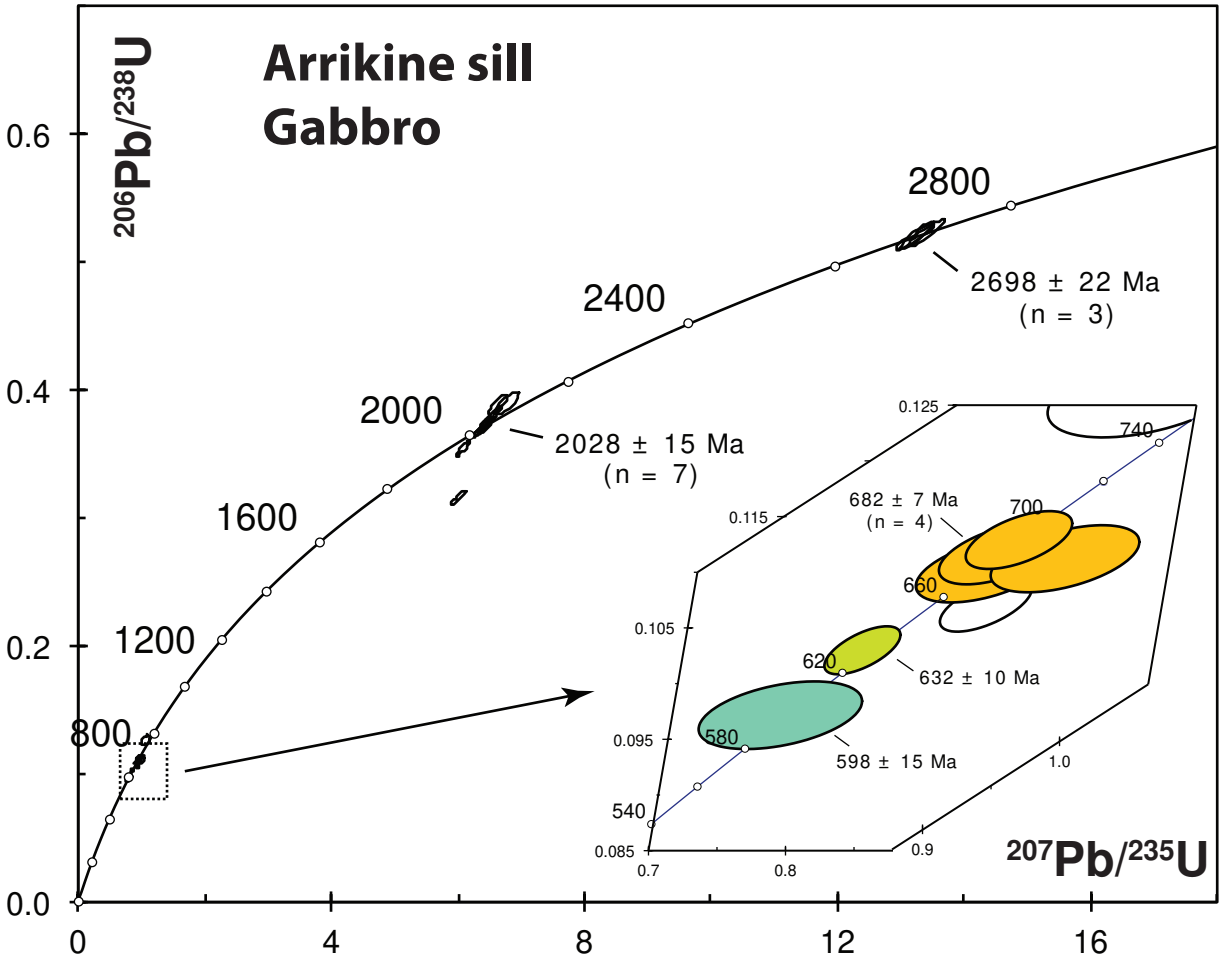

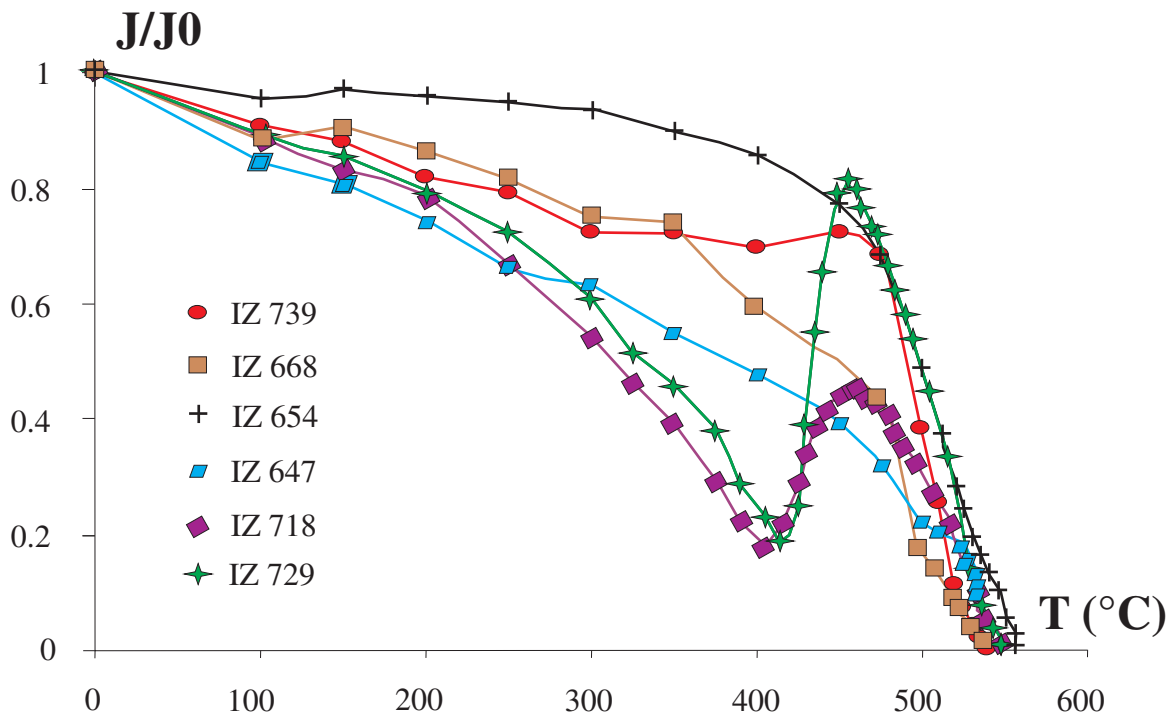
J/J0
1
0.8
0.6
0.4
0.2
0
0
100
200
300
400
500
600
T (°C)
IZ 739
IZ 668
IZ 654
IZ 647
IZ 718
IZ 729

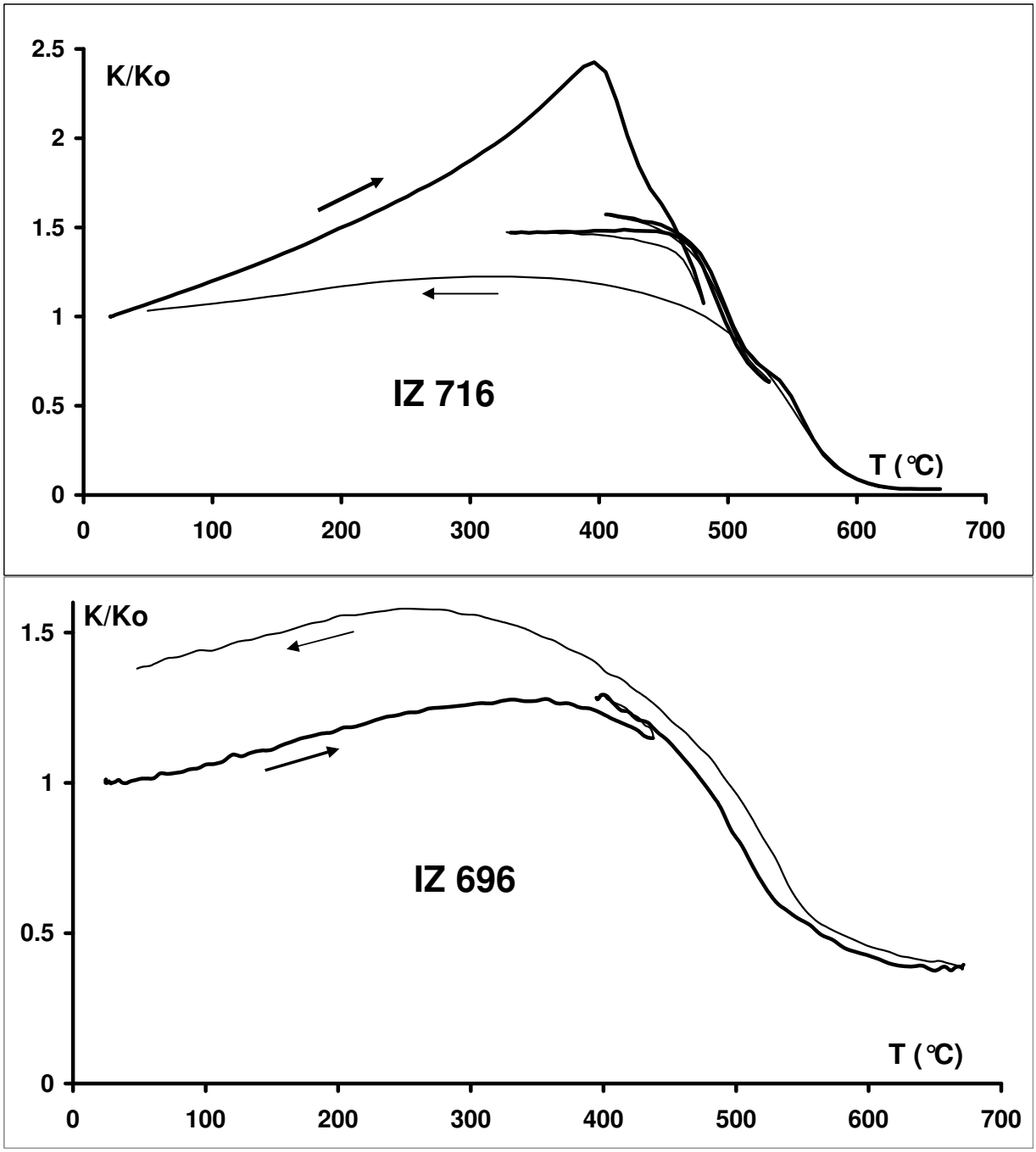
K/Ko
2.5
2
1.5
1
0.5
0
IZ 716
T (°C)
0
100
200
300
400
500
600
700
K/Ko
1.5
1
0.5
0
IZ 696
T (°C)
0
100
200
300
400
500
600
700

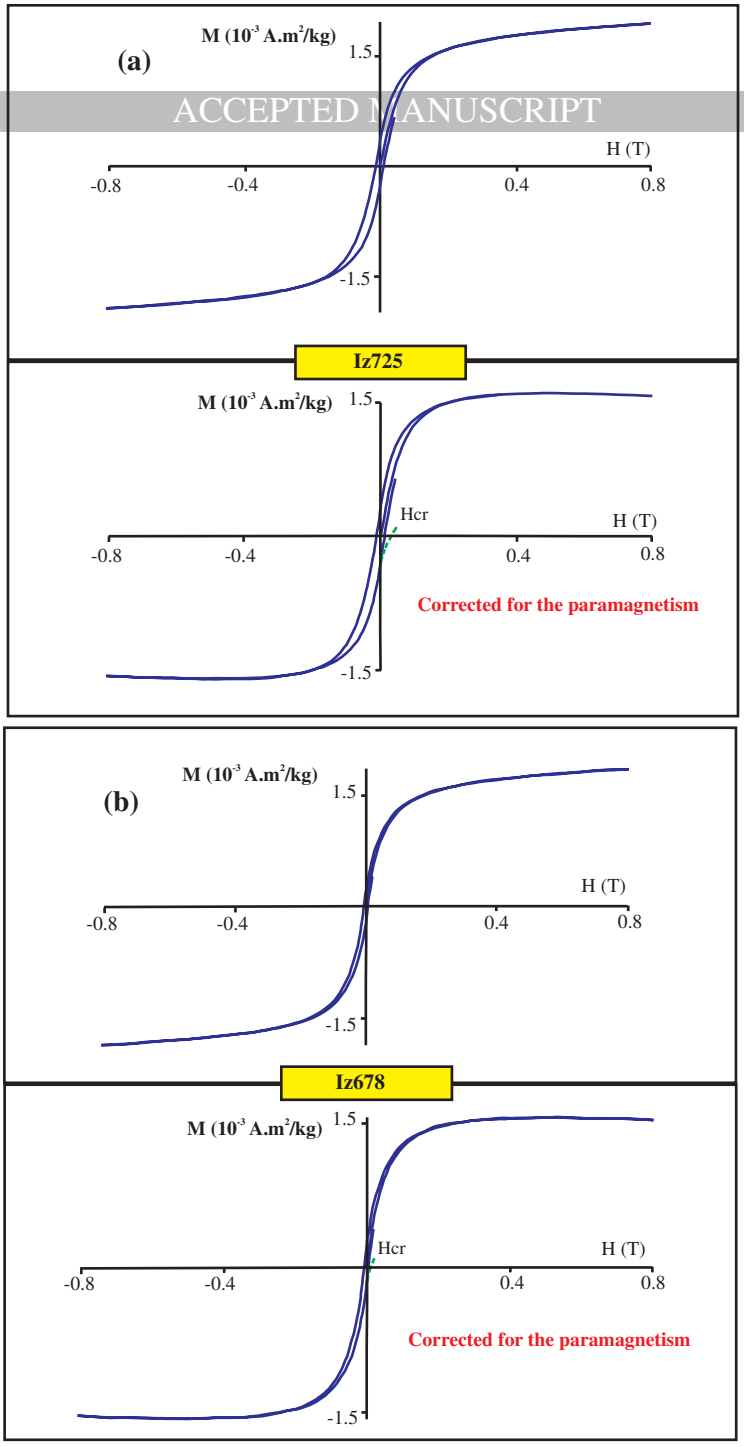

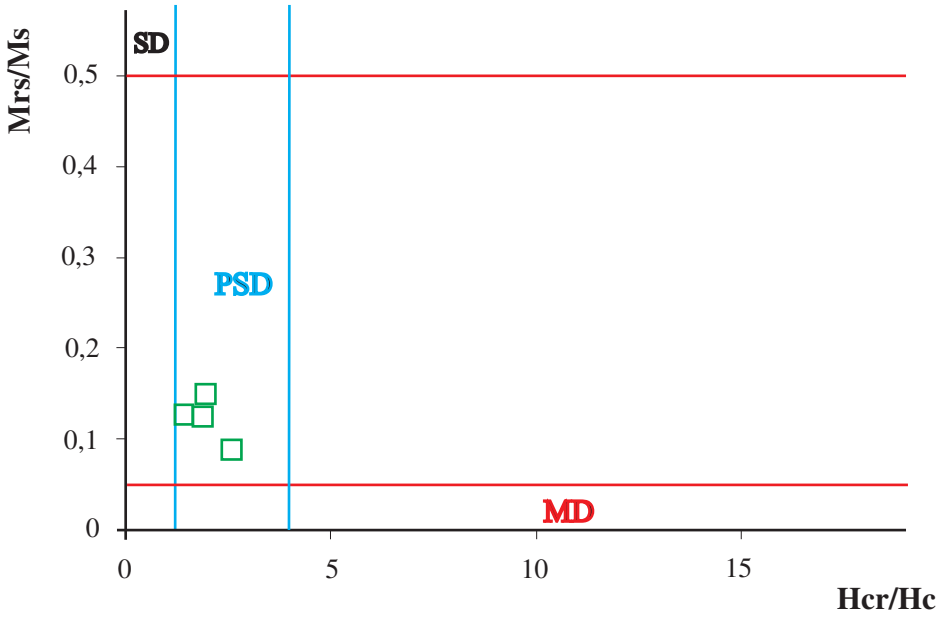

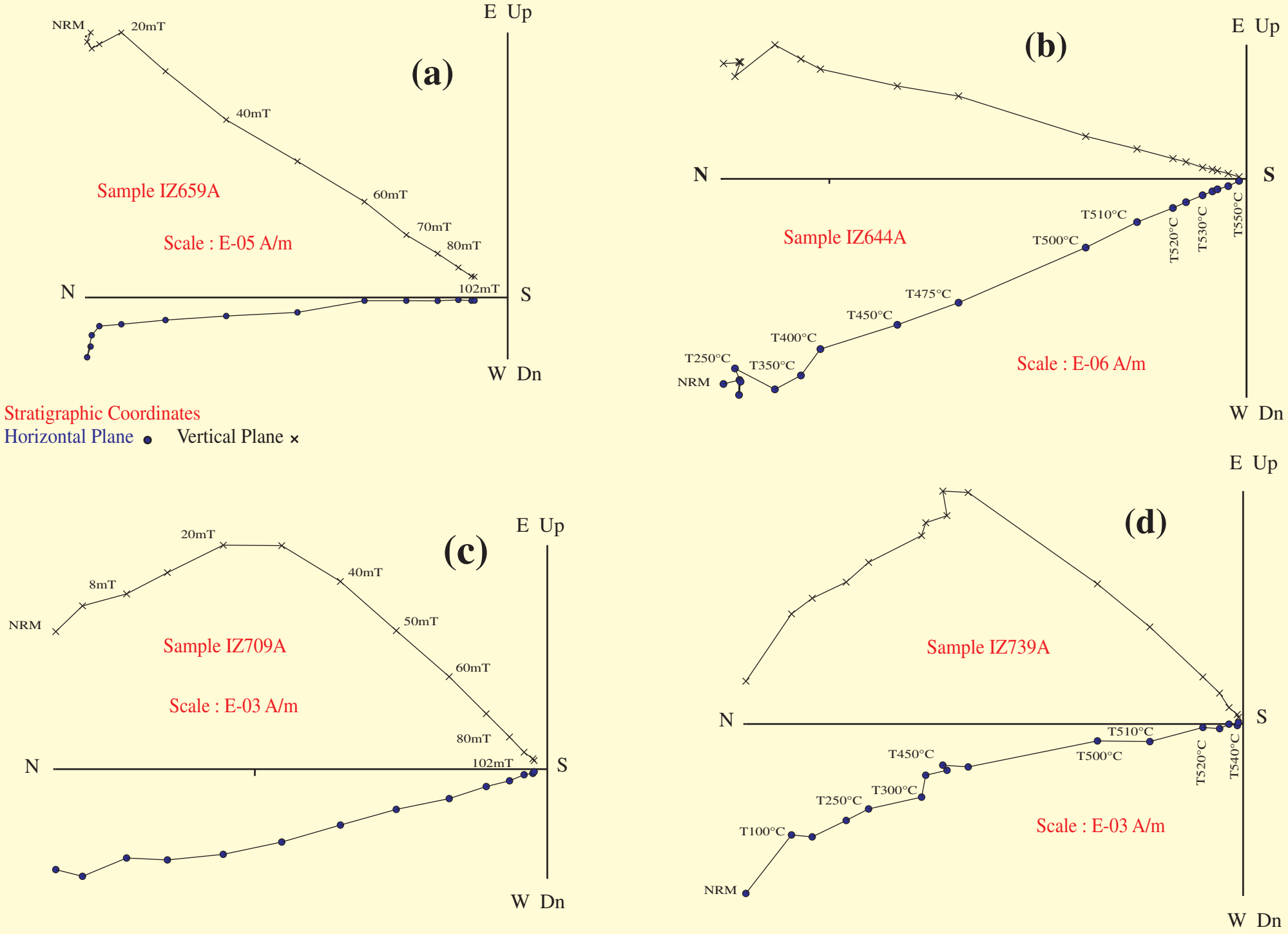

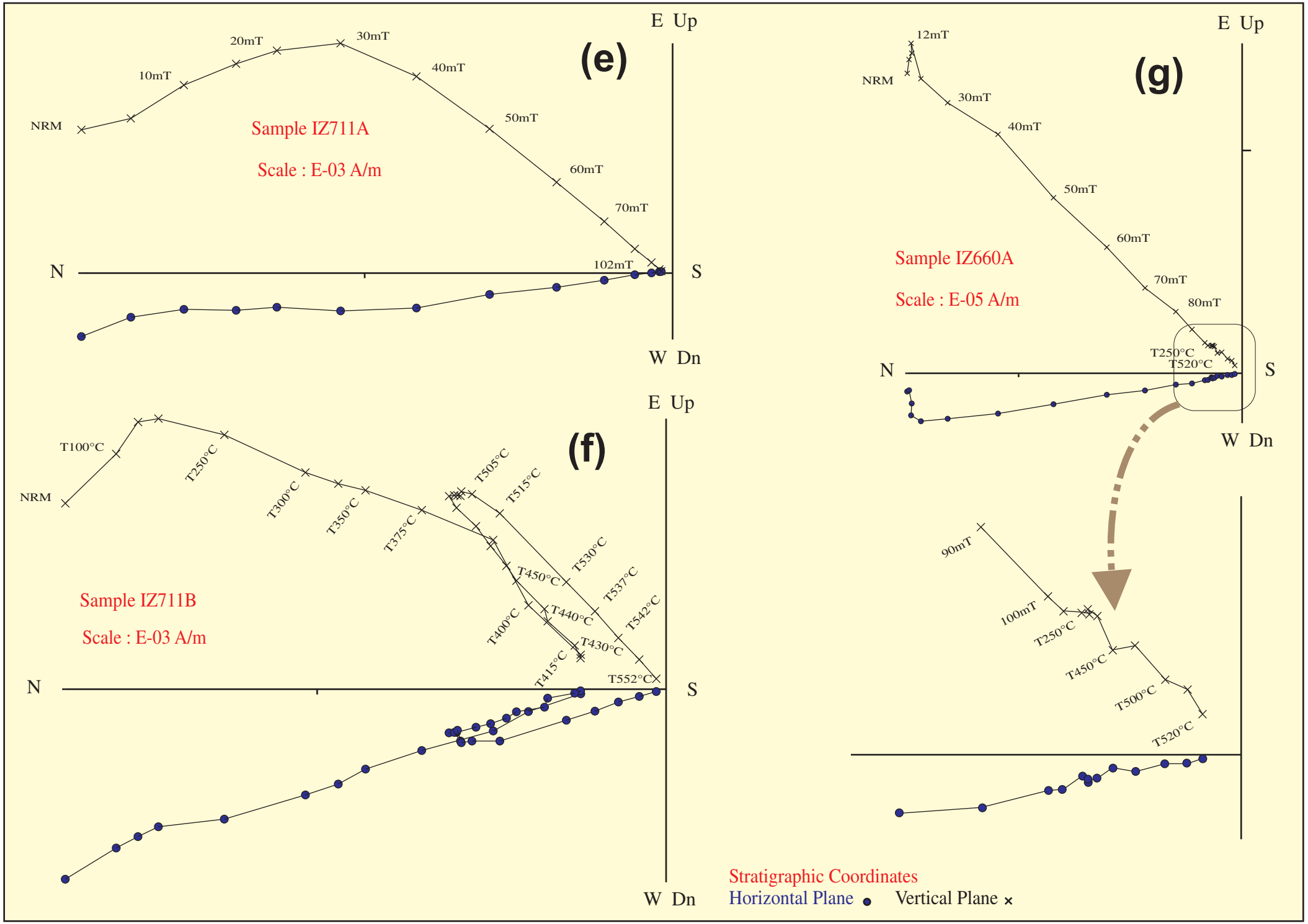

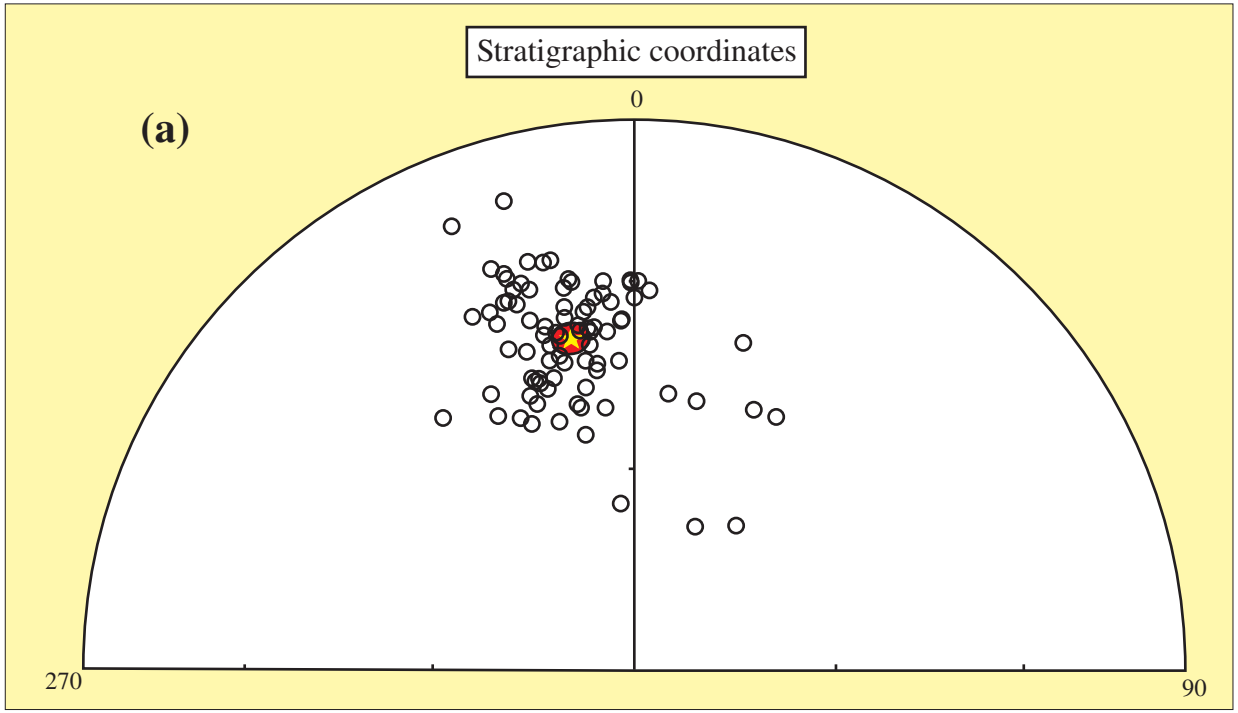
Stratigraphic coordinates
(a)
0
270
90

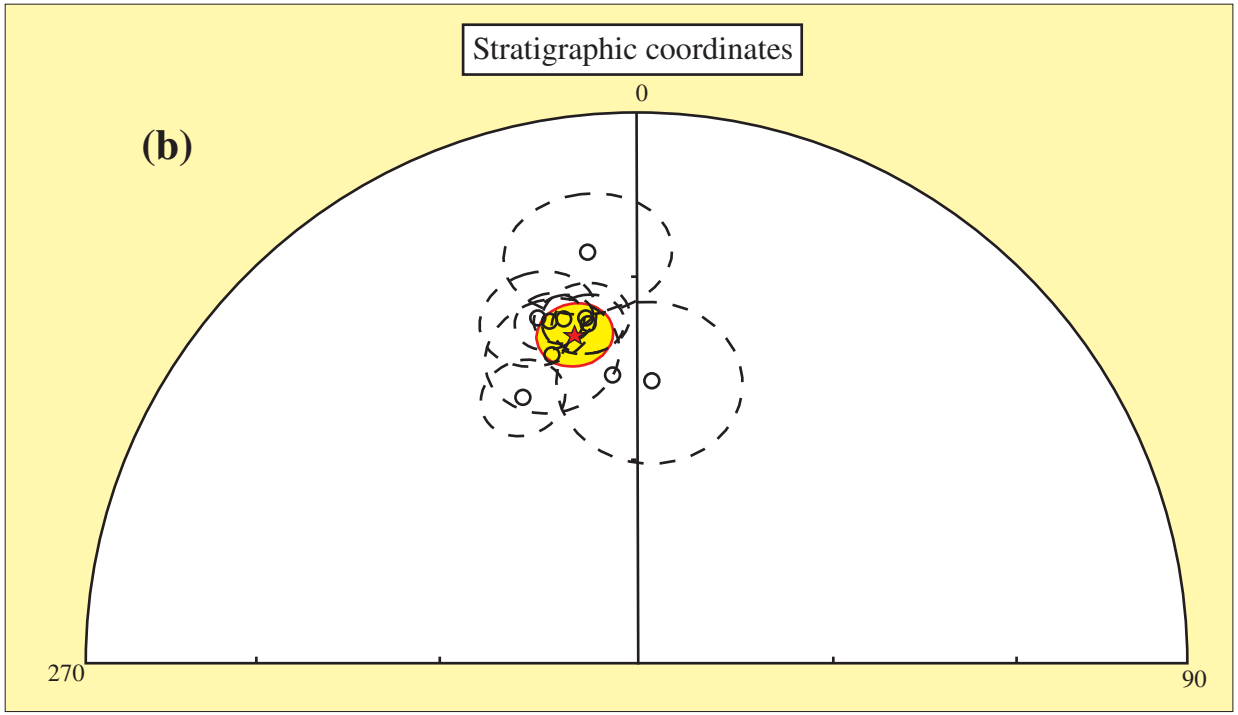
Stratigraphic coordinates
(b)
0
270
90

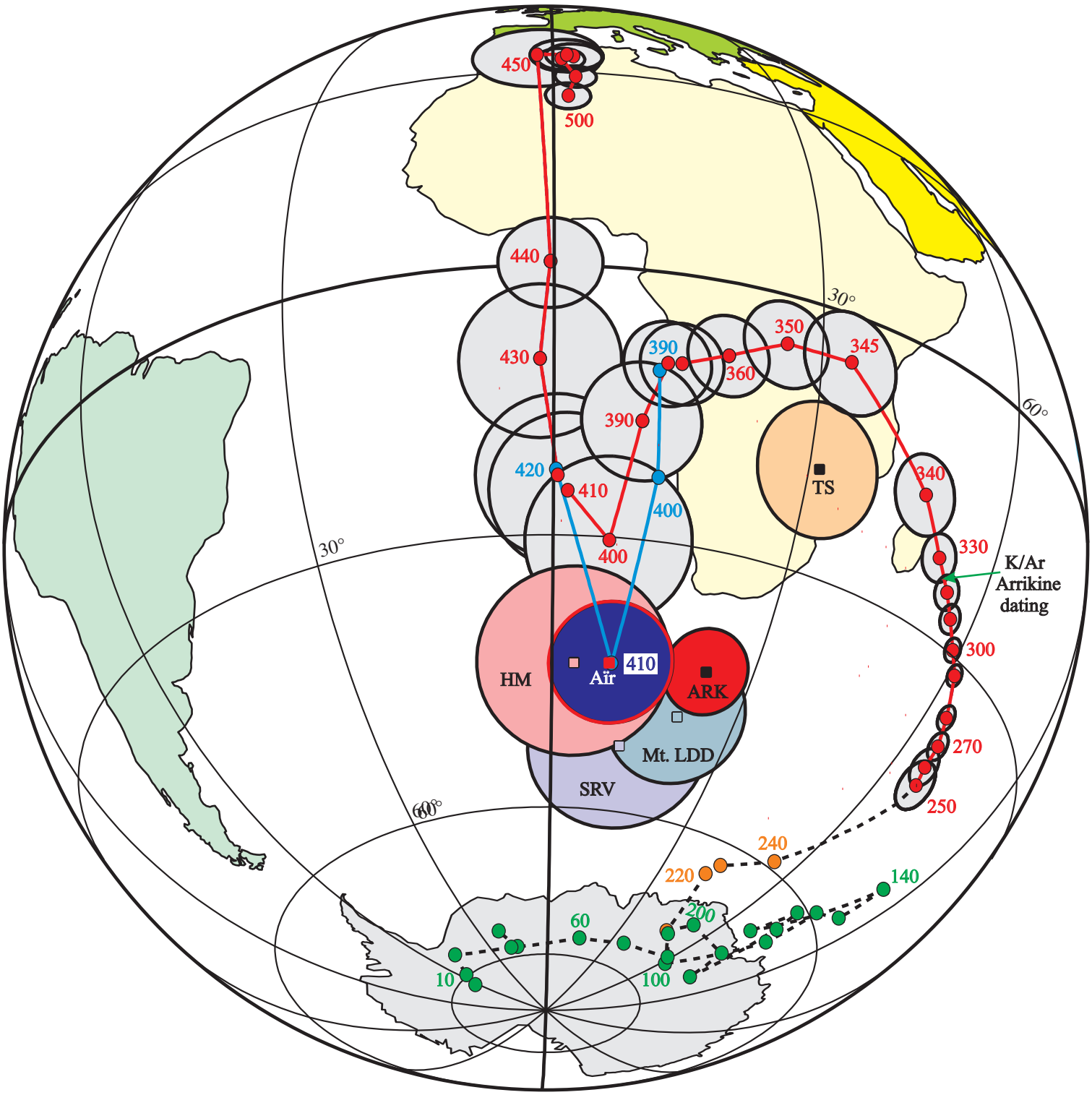
450
500
440
430
390
360
350
345
390
420
410
400
400
340
330
300
270
250
240
220
200
140
100
60
10
TS
HM
Aïr
410
ARK
Mt. LDD
SRV
K/Ar
Arrikine
dating
30°
60°
30°
60°

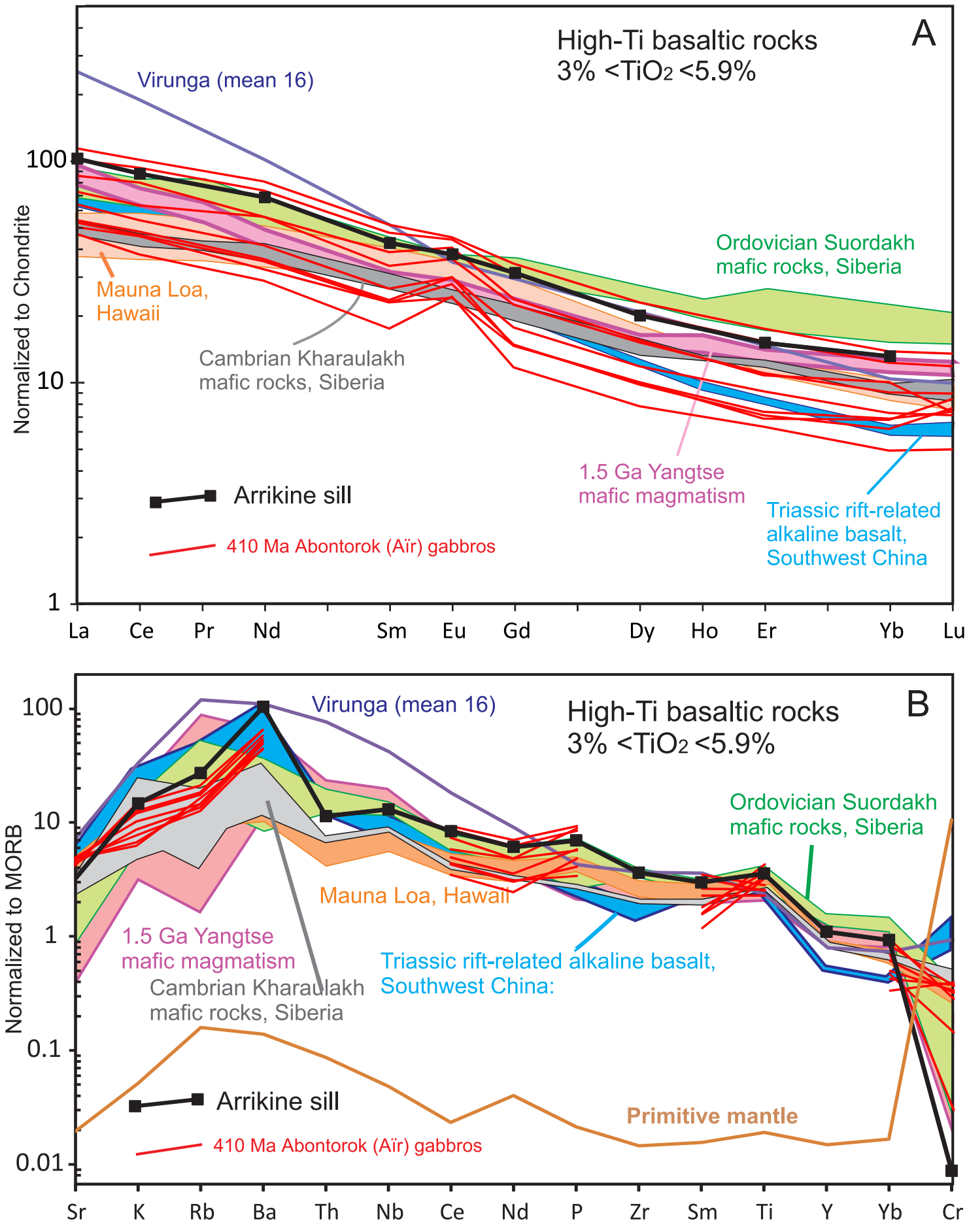
A
High-Ti basaltic rocks
3% <TiO2 <5.9%
Virunga (mean 16)
Ordovician Suordakh
mafic rocks, Siberia
Mauna Loa,
Hawaii
Cambrian Kharaulakh
mafic rocks, Siberia
1.5 Ga Yangtse
mafic magmatism
Triassic rift-related
alkaline basalt,
Southwest China
Arrikine sill
410 Ma Abontorok (Aïr) gabbros
Normalized to Chondrite
100
10
1
La Ce Pr Nd Sm Eu Gd Dy Ho Er Yb Lu
B
High-Ti basaltic rocks
3% <TiO2 <5.9%
Virunga (mean 16)
Ordovician Suordakh
mafic rocks, Siberia
Mauna Loa, Hawaii
1.5 Ga Yangtse
mafic magmatism
Cambrian Kharaulakh
mafic rocks, Siberia
Triassic rift-related alkaline basalt,
Southwest China:
Primitive mantle
Arrikine sill
410 Ma Abontorok (Aïr) gabbros
Normalized to MORB
100
10
1
0.1
0.01
Sr K Rb Ba Th Nb Ce Nd P Zr Sm Ti Y Yb Cr

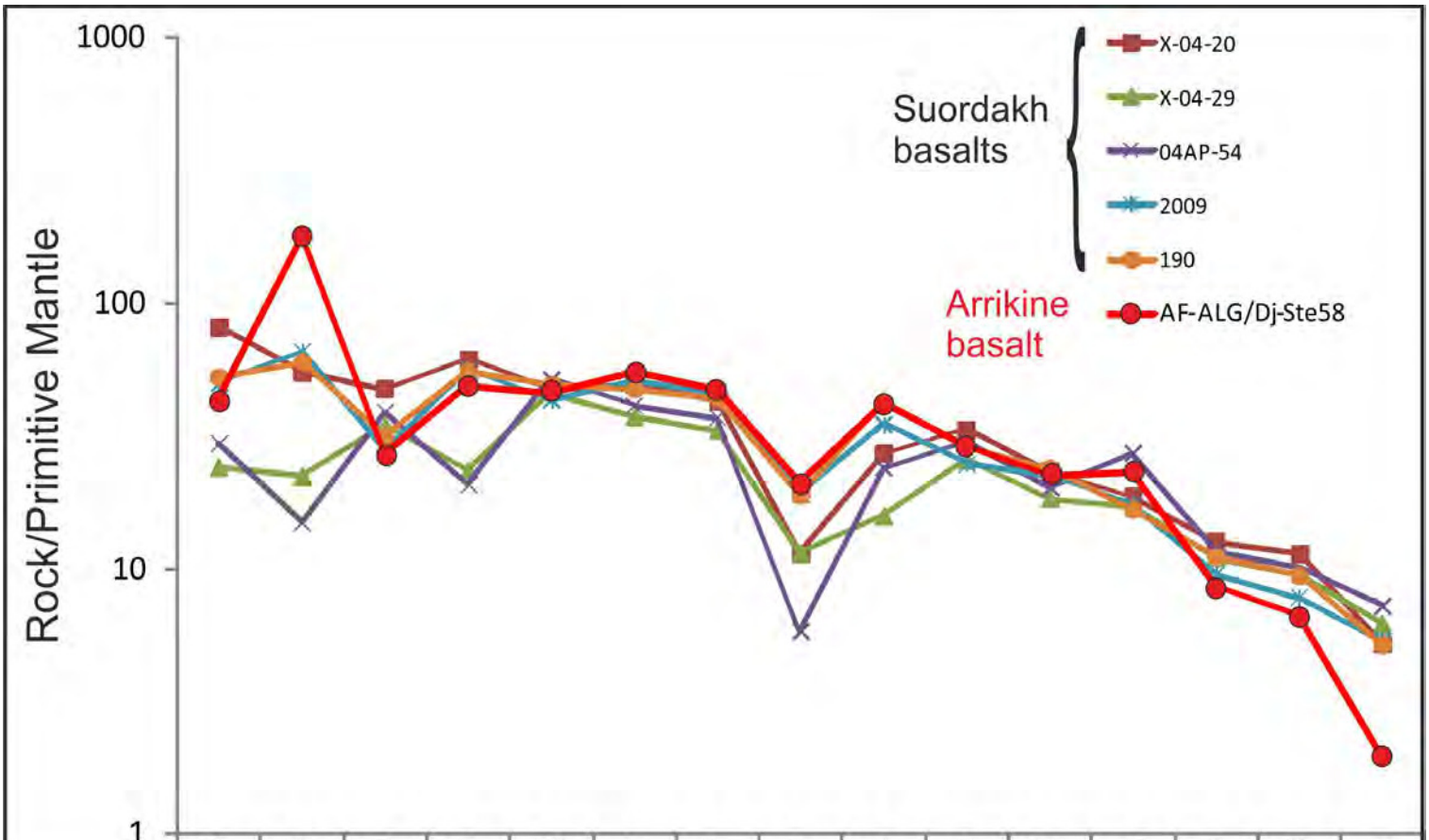

	Rb	Ba	Th	K	Nb	La	Ce	Sr	P	Zr	Sm	Ti	Y	Yb	V
X-04-20	81.26	55.09	47.41	61.37	47.12	49.20	42.76	11.37	27.00	33.48	23.20	18.66	12.62	11.44	5.21
X-04-29	24.09	22.18	34.71	23.49	46.00	37.26	33.18	11.37	15.75	25.71	18.36	17.13	10.99	9.51	6.22
04AP-54	29.61	14.88	38.71	20.71	51.61	41.05	36.90	5.78	23.91	30.00	20.14	27.13	11.69	10.12	7.24
2009	49.92	65.39	27.88	56.16	43.20	50.95	45.92	19.05	34.82	24.82	22.48	17.44	9.49	7.79	5.37
190	52.44	59.81	31.53	55.00	49.37	47.31	43.89	18.91	42.40	28.84	23.87	16.71	11.05	9.41	5.16
AF-ALG/Dj-Ste58	42.83	178.49	26.84	48.97	45.90	54.88	47.34	20.94	41.74	28.60	22.23	23.11	8.48	6.62	1.97

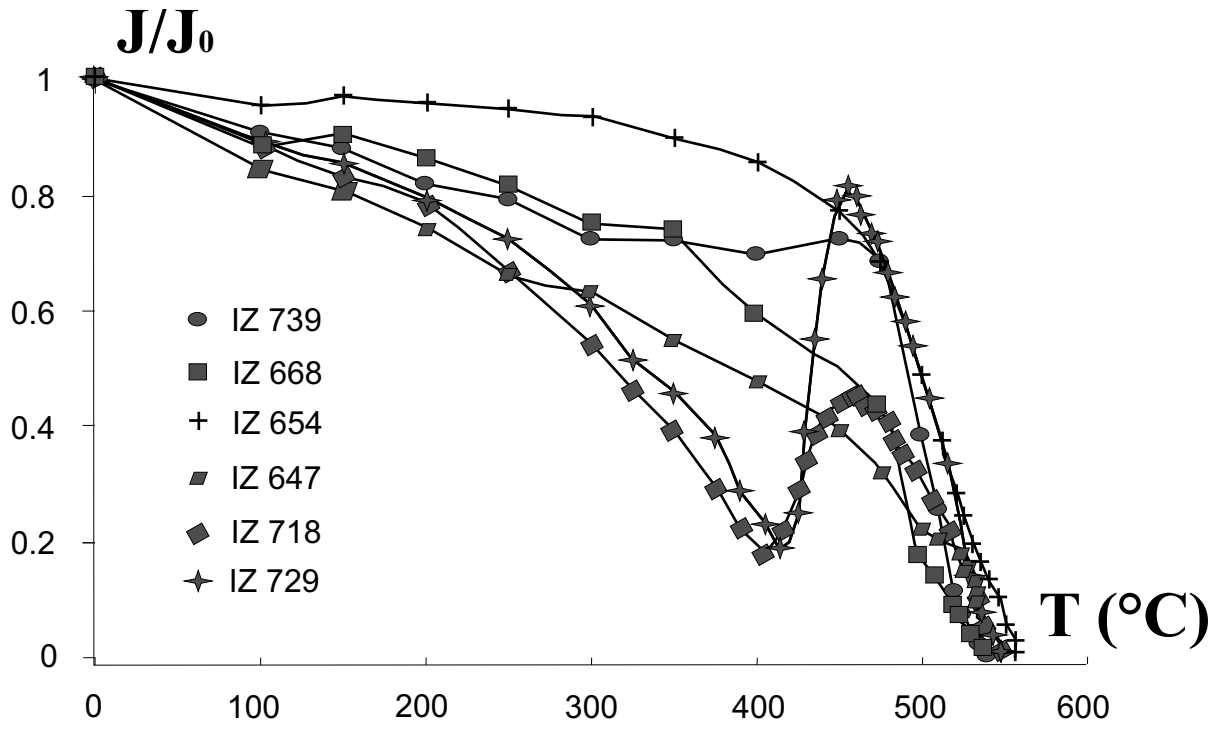
J/J0
1
0.8
0.6
0.4
0.2
0
0
100
200
300
400
500
600
T (°C)
IZ 739
IZ 668
IZ 654
IZ 647
IZ 718
IZ 729

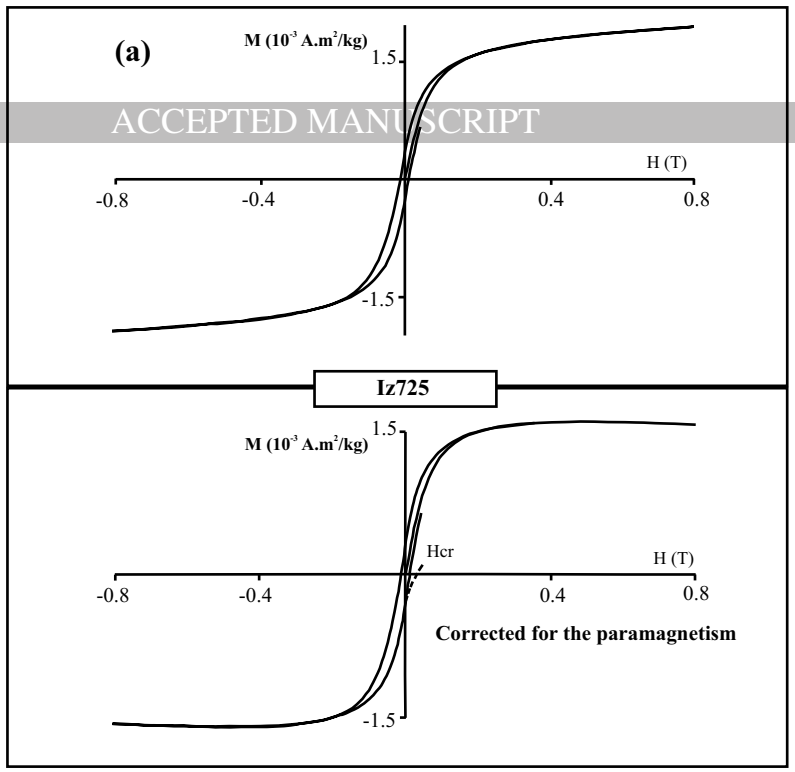

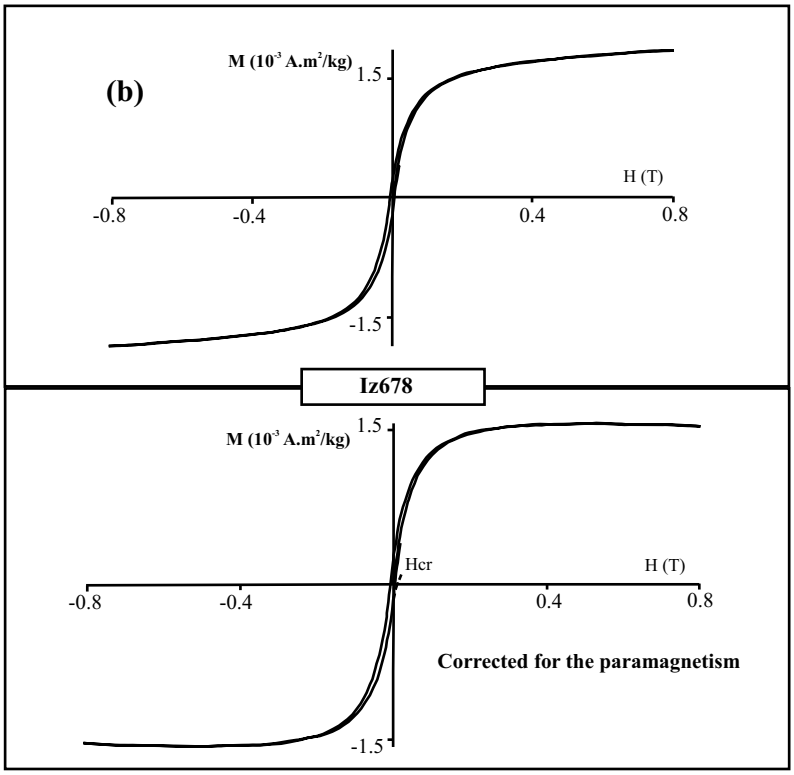

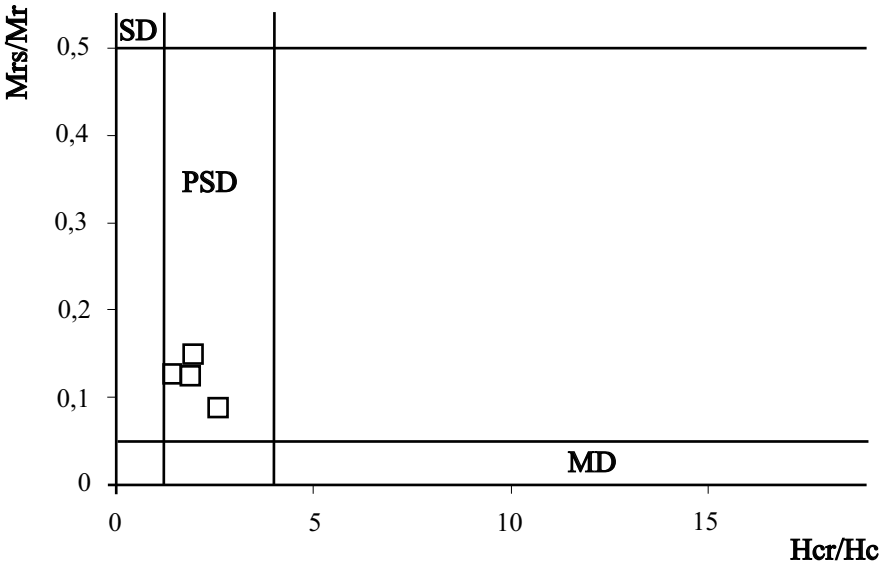

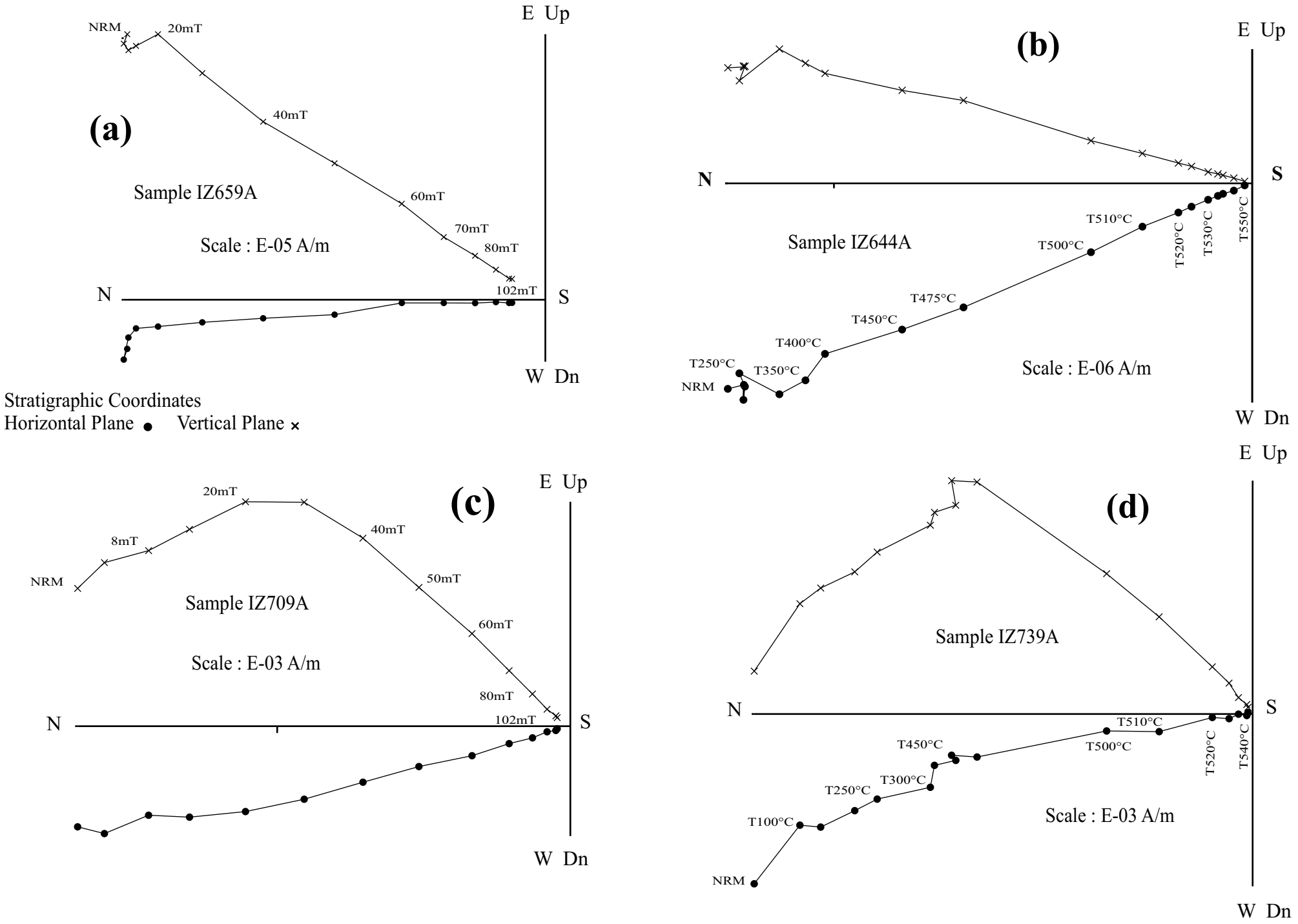

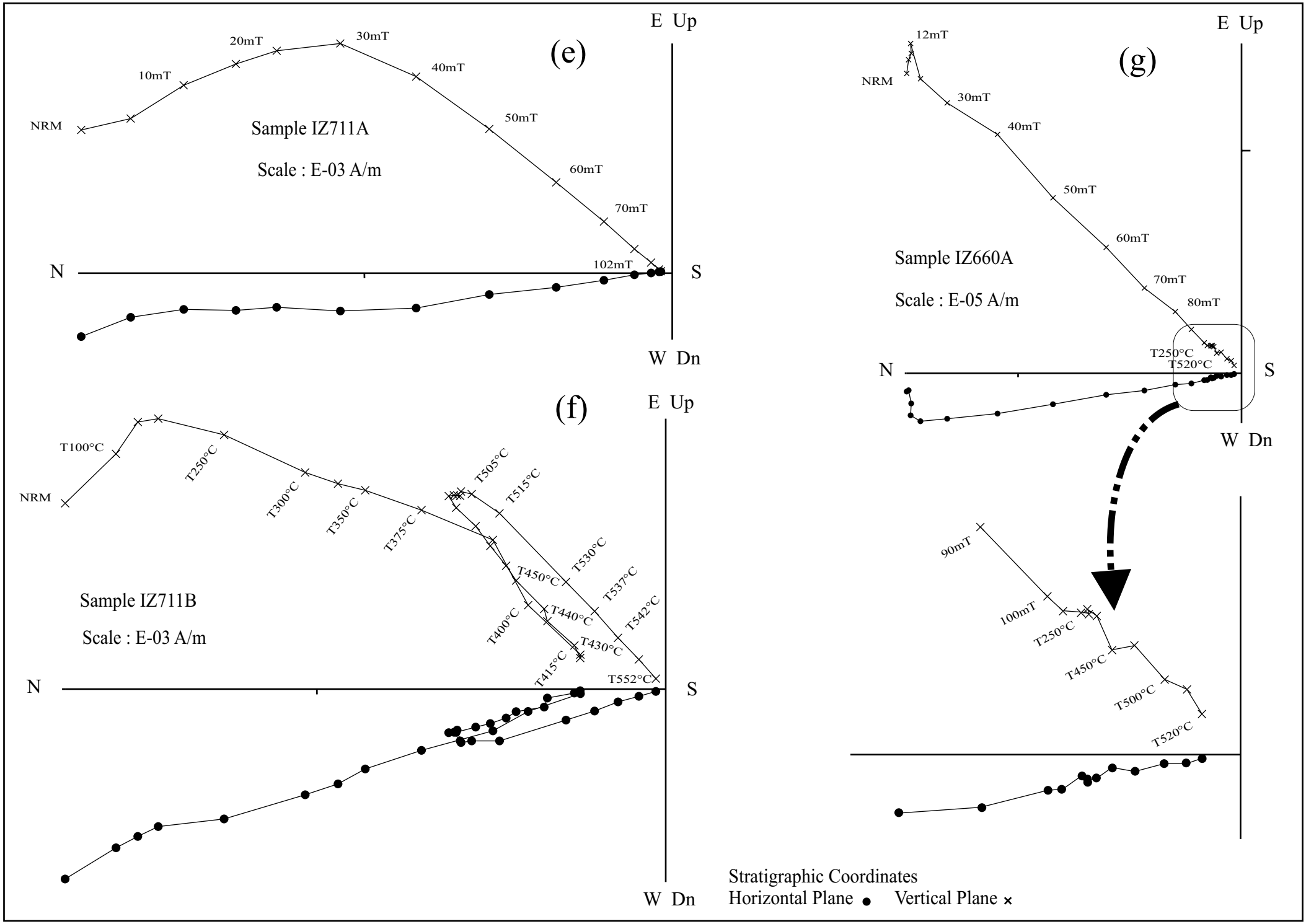

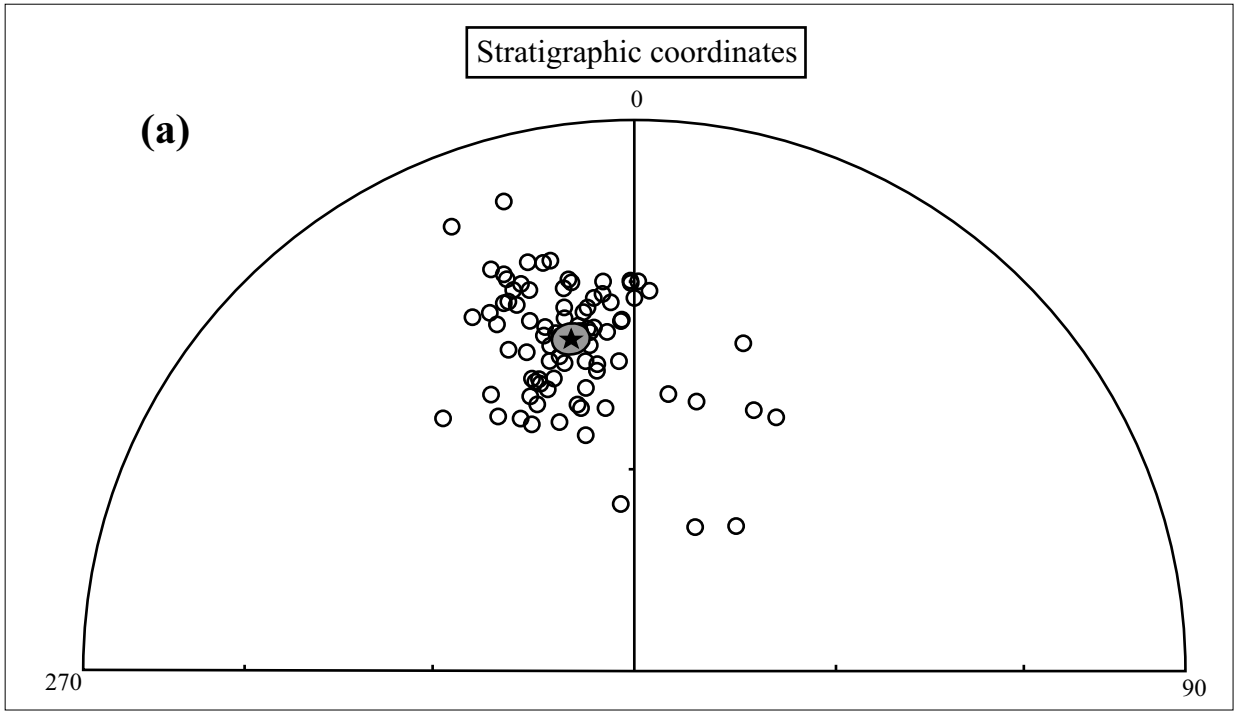
Stratigraphic coordinates
(a)
0
270
90

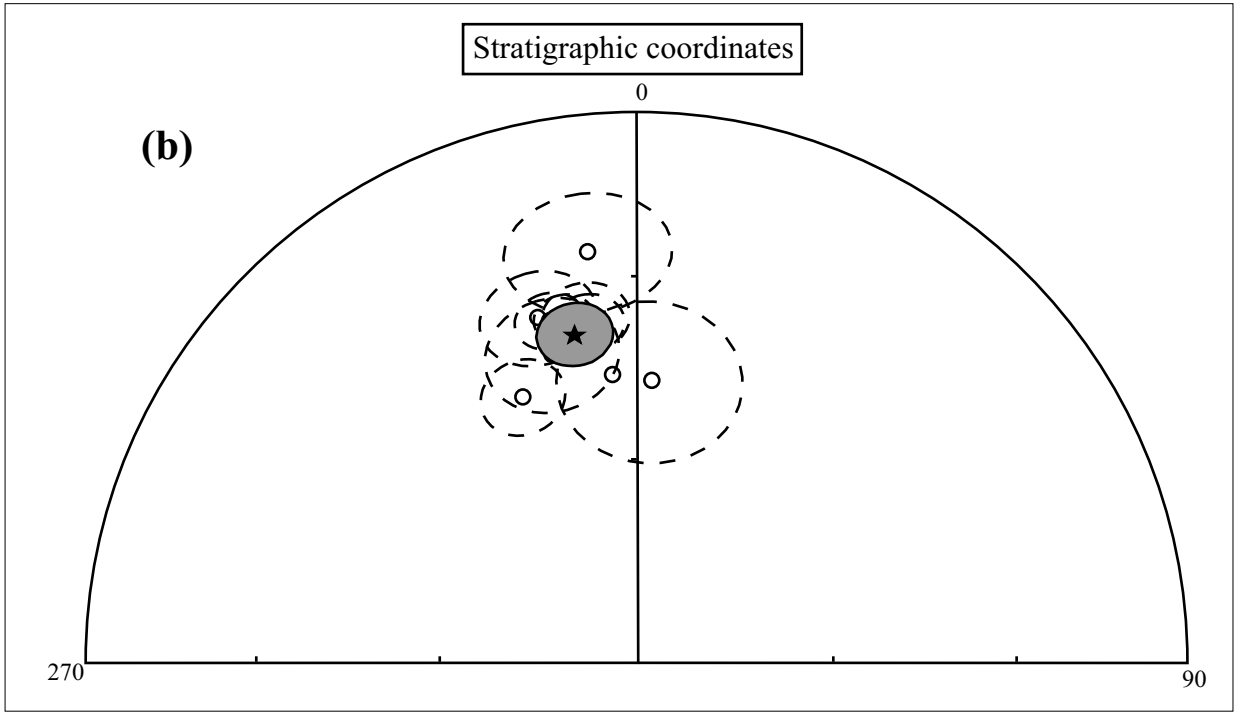
Stratigraphic coordinates
(b)
0
270
90

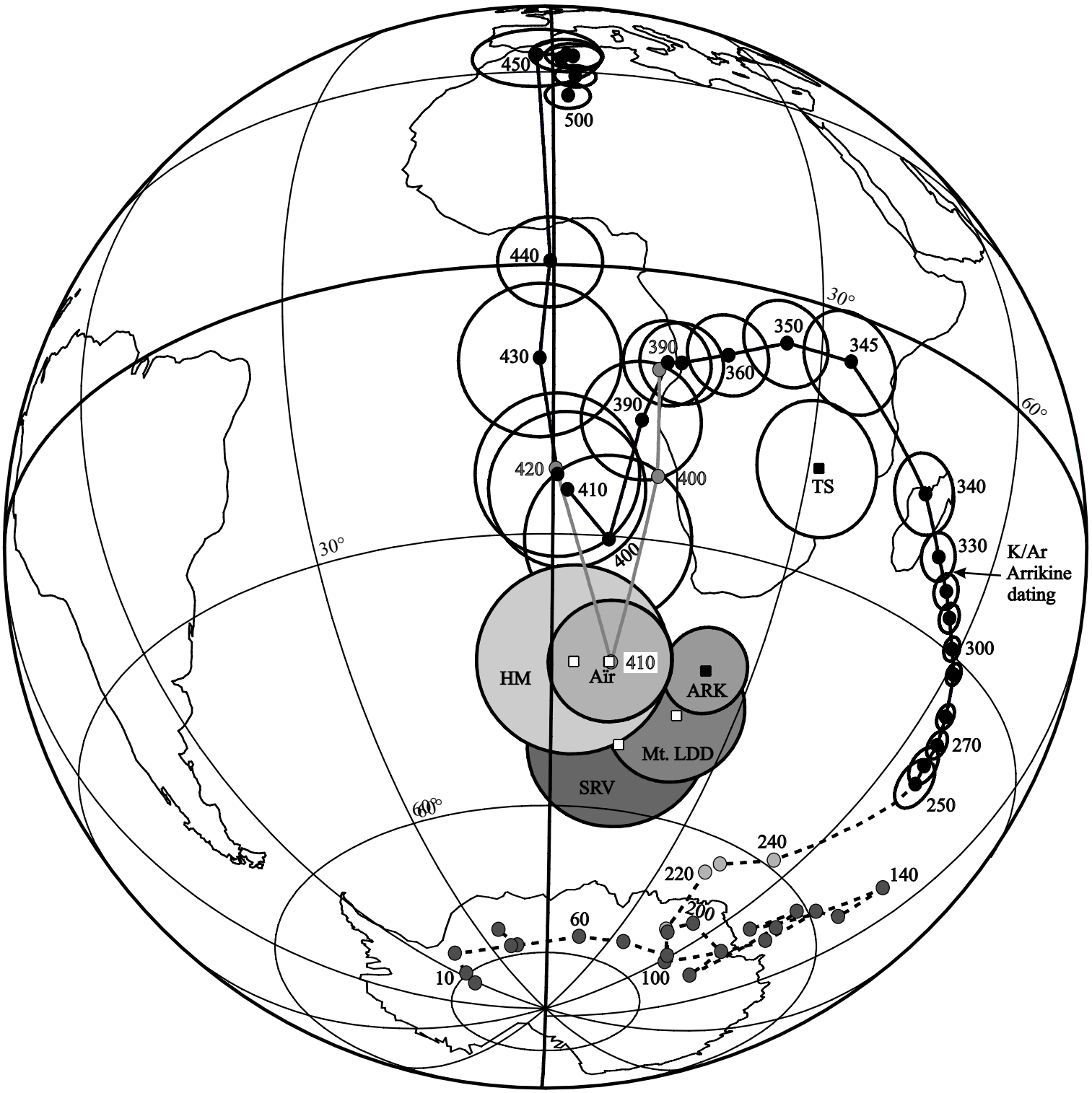
450
500
440
430
390
360
350
345
390
420
410
400
400
TS
340
330
K/Ar
Arrikine
dating
300
270
250
240
220
200
140
60
10
100
HM
Air
410
ARK
Mt. LDD
SRV
30°
60°
30°
60°

A large mafic sill has been discovered in western border of the Murzuq basin
Emplacement age around 410Ma has been obtained by paleomagnetic dating
Emplacement is related to reactivation of mega-shear zones at cratons boundaries
Obtained K/Ar age is that of a rejuvenation attributed to aplitic fluid percolation
These ages correspond to that of the Caledonian and Hercynian unconformities